Sveriges lantbruksuniversitet
Swedish University of Agricultural Sciences

Department of Soil and Environment

Modelling the water balance of a grassland soil

Elvin Rufullayev

Modelling the water balance of a grassland soil

Elvin Rufullayev

Archiving and publishing

Approved students' theses at SLU are published electronically. As a student, you have the copyright to your own work and need to approve the electronic publishing. When you have approved, metadata and full text of your thesis will be visible and searchable online. When the document is uploaded it is archived as a digital file.

Abstract

Expected future climate change characterized by higher temperatures and more frequent summer droughts may cause significant changes in soil hydrological processes leading to limited nutrient and water availability and reductions in plant growth. Soil hydrological and plant growth models attempt to reproduce the complex interactions in the plant-soil water system in terms of mathematical equations, parameters and coefficients. If these models are able to capture the behaviour of the plant-soil-atmosphere continuum, in terms of soil water fluxes in the vadose zone and plant growth, they could help users to understand and predict the effects of climate change.

In the scope of this study, a numerical soil water balance model was applied to three soil lysimeters located in Rollesbroich, Germany to analyse the accuracy of model predictions for temperate grassland. The model output showed some differences in calibrated model parameters and goodness-of-fit for the three lysimeters with identical soil profiles. The numerical analysis of the simulated results showed a satisfactory degree of model plausibility with R^2 values between 0.52 and 0.99, RMSE between 0.01 and 0.05 $cm^3\,cm^{-3}$ for water contents and 0.067 to 0.072 $cm\,d^{-1}$ for actual evapotranspiration. The graphical model analysis showed a good explanation of the main seasonal patterns in the observations, despite some errors revealed by an analysis of the model residuals. It can be concluded that, with some additional improvements, this soil hydrological model could be applied to simulate the effects of future climate change scenarios.

Keywords: calibration, high precision weighing lysimeter, numerical modelling, plant growth, potential evapotranspiration, soil processes, temperate grassland, TERENO, vadose zone, validation.

Popular science summary

Quantification of the soil water budget is important for agricultural and hydrological modelling. It was projected that future climate change would lead to an increased number of dry days in Europe. Thus, the exact quantification of the soil water budget is important to reduce crop yields under expected frequent drought conditions. Besides, knowledge of soil water budget allows predicting the risk of flooding under expected extreme rainfall events due to the limited water holding capacity of the soil.

Measured evapotranspiration and precipitation are prone to errors with standard measurement devices for various reasons, whereas it is complicated to measure percolation of soil water at depth in field soils. Soil lysimeters can measure changes in soil water budget through measurement of evapotranspiration, precipitation and percolation with higher precision than other techniques. Lysimeters consist of an undisturbed soil profile located within a tank with installed measurement devices to quantify the changes in the soil water budget.

Science allows to approximate complex soil-plant-atmosphere interactions with mathematical equations and model parameter values through modelling software. However, best model parameters that are needed to satisfyingly reproduce the observed data are not known initially which requires mathematical algorithms to get a better fit to observations by the model. Model calibration accounts for finding the best model fit to observations through numerous simulations with different combinations of the parameter values. Thus, the numerical model was applied to three soil lysimeters located in Rollesbroich, Germany with six years of measurements to assess the accuracy of model predictions.

The model used in this study considered plant and root growth, water fluxes in the soil and root water uptake. The model results showed a good fit to the observations measured by soil lysimeters after statistical analysis of the best model fit. The results suggested that a high number of model simulations is needed in order to increase the possibility to find the best set of parameters needed to describe the observations. Application of sensitivity analysis in future is needed to find the sampled range of parameter values as well as necessary model parameters which should be included into calibration to get a better fit to observations. Moreover, it is suggested to test the model in a drier climate in order to investigate the main advantage of the applied model which accounts for the root water uptake from the deeper soil layers under drought conditions when the plant available water in the surface layers is exhausted. Such improvements would allow simulating the grass growth under expected future climate change scenarios with drier climate conditions.

Table of contents

Abbreviations

AWAT	Adaptive Window and Adaptive Threshold filter
ET	Evapotranspiration
EC	Eddy covariance
FAO	Food and Agriculture Organization
GA	Generic algorithm
GRG	Generalized reduced gradient
LAI	Leaf area index
MAE	Mean absolute error
MCS	Monte Carlo simulation
MLR	Multivariate ordinary linear regression model
MVG	Mualem-van Genuchten model
NPP	Net primary productivity
RMSE	Root mean squared error
SLA	Specific leaf area
SSE	Sum of squared errors
TDR	Time domain reflectometry
TERENO	Terrestrial Environmental Observatories
WUE	Water-use-efficiency

1. Introduction

Expected changes in climate conditions will affect soil water storage, water and nutrient uptake by roots, plant growth and carbon (C) cycling. This means new challenges in environmental research concerning adaptation of soil management and agricultural practices to account for changing environmental conditions.

Climate change consequences and increase in carbon dioxide (CO_2) emissions by 2050 in Europe would lead to a slight increase in yields in northern Europe and increased drought periods and yield reductions for Mediterranean region (Alcamo *et al.* 2007). On the other hand, increase in temperature by 2 °C would lead to a decline in crop yields (Easterling *et al.* 2007) and several climate change scenarios for Europe confirmed increase of temperature by 2 °C in 2050 (Giorgi and Lionello, 2008). For most climate change scenarios, annual mean precipitation is expected to increase in northern Europe with a greater increase during winter, while in southern Europe the precipitation would decrease with a greater decrease in summer (Olesen *et al.* 2011). It was projected that the number of dry days in the region of study (Rollesbroich) would increase by 2050 under a projected increase in temperature of 1.5 °C (Trnka *et al.* 2011). Such a change in climate would require farmers to adapt by changing the sowing harvest dates for most of the crops.

According to Olesen *et al.* (2011) grassland was considered the crop least affected by future climate change as the number of growing days would increase and the damage caused by frosts during the winter season would decrease. However, extreme climate events, such as a higher frequency of drought during the summer, soil erosion and heat stress are expected to have significant impacts on grassland in all zones of Europe. The response of grassland to climate change would depend on soil type, management strategies and species composition. Chang *et al.* (2017) found that under future climate projections, the growing season of grassland in western Europe would end earlier leading to a decrease in productivity related to drought conditions in mid-summer. In addition, higher productivity of grassland during the spring followed by water stress of the grass in summer was explained by increased soil water depletion during the warm spring and earlier onset of leaf growth as a result of decreased precipitation during summer and increased temperatures. Furthermore, Morecroft *et al.* (2004) showed that winter precipitation had no effect on grassland productivity, which was mainly controlled by summer precipitation in the current and previous years which implies that the expected increase of precipitation in northern Europe under changing climate would not give significant advantages, since summers are expected to be drier. Field experiments have also found a similar decline in productivity of temperate grassland under warming and dry soil conditions (Boeck *et al.* 2007, 2008). An experiment conducted on Swiss grasslands showed no response to summer drought but the sites

with low annual precipitation were more vulnerable to drought conditions compared to the sites with higher precipitation (Gilgen and Buchmann, 2009). In addition, plants adapt to the limited water use to avoid stress caused by drought during later stages of the growth through changes in crop phenology (Francia *et al.* 2011). However, water saving by plants at early growth stages has disadvantages such as increased evaporation from the soil surface (Condon *et al.* 2004).

Accurate and precise measurement and monitoring of soil water fluxes in the unsaturated zone is required to help us better understand the impacts of changing climate conditions on soil and plant processes. Correct estimation of soil water content and actual evapotranspiration (ET_a) is a primary issue in food security, agricultural management and crop growth. Precipitation, percolation, surface runoff and ET_a determine changes in the soil water content. Drainage and surface runoff may account for up to 50% of total water losses from incoming precipitation while evaporation is climate and soil dependent and may account up to 35 % losses of soil water (Wallace, 2000). Varying soil water content strongly impacts the crop productivity, soil surface energy and runoff dynamics (Vinnikov *et al.* 1999). Timely identification of periods of low soil moisture content in crop yield modelling is crucial to warn farmers about the necessity of irrigation (Heathman *et al.* 2003). Soil water content modelling could also help to predict the risk of flooding when the soil is completely saturated and is unable to retain more water leading to surface runoff with subsequent soil erosion (Zheng, 2006).

Precipitation measurement is one of the most important parts of any hydrological study. However, rain gauges which are standard method of precipitation measurement are prone to high errors due to the deformation of the wind field (Sevruk, Hertig and Spiess, 1991), evaporation and wetting losses (Strangeways, 1996; Yang *et al.* 1999), splashing of raindrops (Strangeways, 1996) and high errors during the wintertime due to snow and frost (Sevruk, 1996). This leads to issues in precise calculation of soil water balance (Kampf and Burges, 2010).

One of the most direct methods of measuring actual evapotranspiration with low operational costs and high resolution is eddy covariance (EC) which determines the exchange of water and gases between soil and atmosphere (Gebler *et al.* 2015). However, under limited thermal and mechanical turbulence, eddy covariance tends to underestimate the fluxes (Li *et al.* 2008) leading to a deficit in the energy balance of between 20 and 25% (Hendricks Franssen *et al.* 2010). Therefore, actual evapotranspiration estimated from the eddy covariance method tends to be strongly underestimated.

Actual evapotranspiration could be estimated from the measurement of the soil water contents by time domain reflectometry (TDR) and precipitation rate if the water fluxes across the bottom boundary of the soil profile could be measured. Application of the soil lysimeters in recent years showed the reliable measurement of the seepage at the boundary condition leading to a precise quantification of the

soil water balance (Meissner, *et al.* 2010). Weighable soil lysimeters, allow to determine fluxes at the lower and upper boundaries of the soil profile with high precision (Meissner *et al.* 2007) and provide a basis for deriving and calibrating models describing soil water flow and solute transport (Wriedt *et al.* 2004). The weighable nature of lysimeters filled with soil cores, allows to quantify precipitation and actual evapotranspiration based on the change in the weight with high resolution of less than 10 g of mass loss, which is equivalent to 0.01 mm of water (Von Unold and Fank, 2008). Actual evapotranspiration measured by soil lysimeters showed a good agreement with the FAO-56 Penman-Monteith estimation method on an hourly basis (López-Urrea *et al.* 2006; Vaughan, Trout and Ayars, 2007). Evett *et al.* (2012) found that corrected actual evapotranspiration (ET_a) estimated by eddy covariance method underestimated ET_a measured by the lysimeter by 18% which was caused by the varying growth of the plants. On the other hand, weighing lysimeters are prone to various errors such as vibrations caused by animals and wind, which can be managed through the application of various algorithms (Peters *et al.* 2014).

Soil hydrological model after the procedure of calibration implying obtaining the best fit to observed data could be used to simulate the plant growth and changes in the soil water balance under drier conditions with the driving data from global and regional-scale climate models predicting expected changes in climate conditions. Root water uptake is an important component affecting changes in soil water balance and plant growth modelling. Many different macro- and microscopic root water uptake models have been developed that allow users to address the complex interactions in the soil-plant system (van Lier, Metselaar and van Dam, 2006). There are several root water uptake models accounting for compensation mechanism (Jarvis, 1989; Li et *al.* 2006; Lai and Katul, 2000). Compensation mechanism implies increased root water uptake from deeper soil layers when the water uptake is reduced in top layers in order to resist the reduction in plant transpiration (Santos *et al.* 2017). According to Santos *et al.* (2017) root water uptake models not accounting for the compensation mechanism, such as Feddes *et al.* (1978) are less accurate in estimation of plant transpiration and soil water contents under drier climate conditions. Soil water fluxes are well-studied but are complex and show non-linear nature and it can be difficult to get input parameters for numerical hydrological models since they depend on various environmental processes quantified with error-prone measurement devices, and mathematically defined uncertain model parameters. Manual adjustment of the various model parameters especially with large timescale is beyond the human capabilities. Calibration of the soil hydrological model could help to explain complexity of soil hydrology through large amount of simulations with varying model parameters to get the best fit of modelled variables to observations.

Assessment of plant-available water in deeper soil layers is important to evaluate potential risks of impacts on soil ecosystem services due to global water shortages caused by changes in climate conditions (Pinheiro, de Jong van Lier and Metselaar, 2018). A combination of soil hydraulic properties and limiting plant water potentials can be used to describe plant water stress through simulation of the critical value of water content or pressure head at which plant water uptake would start to decrease (Raats, 2007). Measurements of soil hydraulic properties and plant water uptake in conjunction with increased power of computing devices and modelling software can help to obtain information about this critical threshold value of water content (Šimůnek, van Genuchten and Wendroth, 1998).

Expected changes in soil hydrology due to future climate change motivated the initiation of the TERENO (TERrestrial ENvironmental Observatories) project in Germany. An experimental lysimeter network (SOILCan) was built to study long-term changes in soil hydrology, carbon and nutrient fluxes into groundwater and the atmosphere under different land use. The focus was on "critical zones", i.e. areas that are already affected or are highly vulnerable to the expected changes in climate (Bogena *et al*. 2012; Zacharias *et al*. 2011; Zebisch *et al*. 2005). In this study, numerical simulations of soil water flow, water uptake and plant growth within the software STELLA Professional were compared with measurements made during an 6-year period in three weighable SOILCan lysimeters located at Rollesbroich within the Rur catchment. A free-derivative optimization algorithm was used to derive parameters of the numerical model. The obtained results from numerical simulation were used to explore the best fit of simulated values to observed data from lysimeter network. Such an analysis is important to draw conclusions regarding the further improvement of the numerical model and the reliability and accuracy of future simulations to be carried out for climate change scenarios.

2. Materials and methods

2.1. Site description

TERENO (TERrestrial ENvironmental Observatories) is a network of lysimeters across Germany under different land uses (Pütz *et al.* 2016) which was established to enable analyses of the effects of climate change at selected sites (Zebisch *et al.* 2005) through translocation of soil lysimeters from their original location to contrasting climates within TERENO network.

The grassland lysimeter station analysed in this project is located at Rollesbroich (50°37'19''N, 6°18'15''E, 511 m a.s.l.) within the Rur catchment. It consists of 6 lysimeters surrounded by intensively managed grassland (Figure 1) (Pütz *et al.* 2016). The plant species composition consists mainly of perennial ryegrass (*Lolium perenne*) and white clover (*Trifolium repens*).
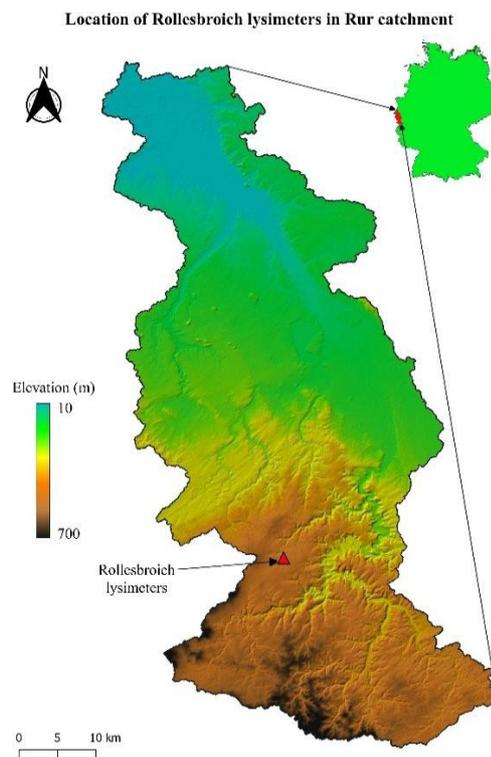
Figure 1. Location of Rollesbroich lysimeters within Rur catchment (data source: NASA JPL, 2013).

The climate in Rollesbroich is humid temperate, with a mean annual precipitation of 1150 mm and a mean annual air temperature of 8 °C. Actual transpiration rates are close to calculated potential transpiration in most years implying only short periods of drought and sufficient amounts of plant available water (Table 1).

Despite the fact that the driest years were 2013 and especially 2018, evapotranspiration values are still comparable with other years.

Table 1. Annual precipitation and evapotranspiration for Rollesbroich lysimeters (2013-2018).

Year	Lysimeter precipitation (mm y⁻¹)			Actual evapotranspiration (mm y⁻¹)*			Potential evapotranspiration (mm y⁻¹)
	Ro-1	Ro-3	Ro-5	Ro-1	Ro-3	Ro-5	
2013	1002	1041	1001	612	633	582	646
2014	1105	1122	1065	683	659	647	689
2015	1155	1185	1146	641	607	626	732
2016	1097	1126	1013	611	592	567	688
2017	1136	1185	1129	619	636	607	718
2018	944	969	931	600	605	582	785

* actual evapotranspiration included gaps of missing data

The soil at the Rollesbroich station is a Stagnic Cambisol with a sandy loam texture in the uppermost (Ah) mineral horizon and with a dominance of sand throughout the whole profile (Figure 2).
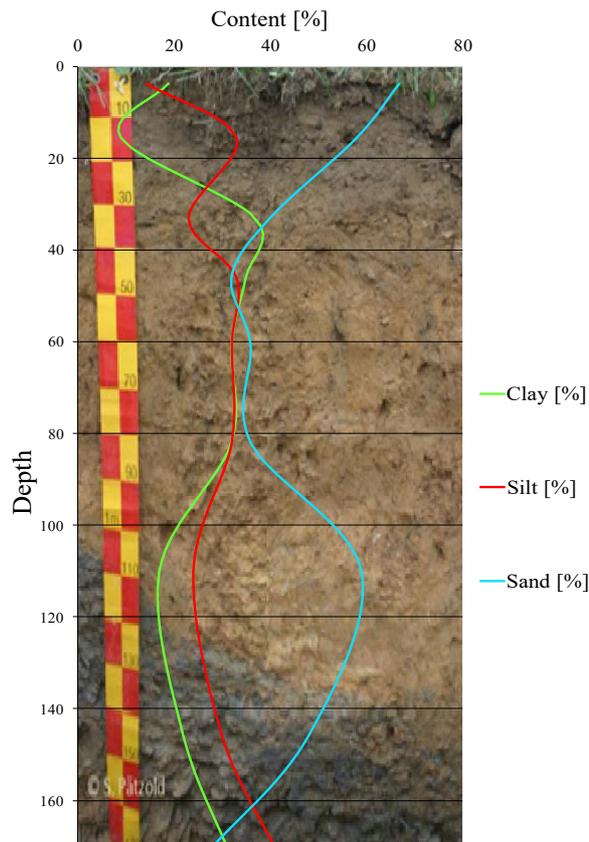
Figure 2. Soil profile of Stagnic Cambisol with textural content of the Rollesbroich lysimeters (provided by Stefan Pätzold).

According to Pütz *et al.* (2016) liquid manure was applied to the lysimeters at the site (~1.6 L/m^2) two to three times per growing season. In addition, three to four cuts of grass per growing season were performed on the lysimeters based on observations of the grass height in the surrounding area.

2.1.1. Lysimeter design

The lysimeter station comprises 6 lysimeters in a hexagonal pattern surrounding a service well in the centre (Figure 3). Such a structure ensures identical experimental and monitoring conditions and therefore comparable results. The lysimeters are housed in porous concrete rings, which leads to thermodynamic equilibrium between the lysimeter and the surrounding soil. The main service well contains infrastructure such as pumps, power supply, measuring transducers, data loggers and modem, sampling bottles and a water tank to collect seepage. The lysimeter walls are made of stainless steel with a surface area of 1 m^2 and depth of 1.5 m.
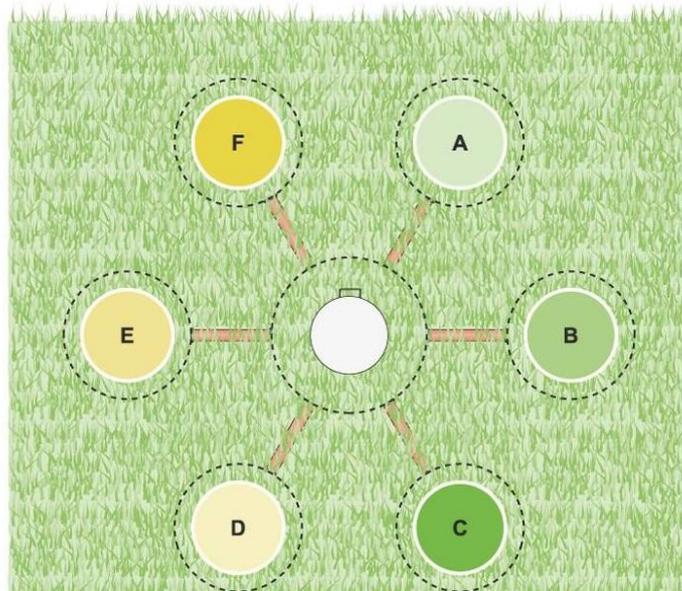
Figure 3. Spatial emplacement of six soil lysimeters around the main service well (provided by UMS AG, München, Germany).

A suction rake with porous tube is installed at the base of the lysimeter at a depth of 1.45 m. Tensiometers, temperature and matric potential sensors, heat flux plates, carbon dioxide gas sampling tubes and suction cups were installed at depths of 0.1, 0.3, 0.5 and/or 1.4 m (Figure 4).

Before the final installation of the lysimeters, three load cells with a 10 g resolution (approximately equal to 0.01 mm of water) were installed at the bottom of each lysimeter. Finally, data loggers, transducers and control units were

connected to probes, sensors and load cells. The seepage water tank was located on a plate with a resolution corresponding to a water amount of 0.001 mm.

Figure 4. View of lysimeter prepared for installation in its housing (left) and suction rake of lysimeter (right) (Pütz et al. 2016).

To avoid artificially affecting water flow conditions in the lysimeter, the matric potential of the lysimeter at the bottom boundary was adjusted to the value measured in the surrounding soil with a tensiometer (Pütz *et al*. 2016). A tensiometer at depth of 1.4 m controls matric potential in the lysimeter, which enables both upward and downward water fluxes across the bottom boundary and therefore adjusts the water dynamics in the lysimeter to the surrounding field conditions. Such a control algorithm of matric potential in different soils transforms the finite soil lysimeter into an "infinite" soil column by pumping water from the lysimeter into the seepage tank in a case of higher matric potential compared to the field conditions and vice versa. Additionally, a weather station was installed next to the lysimeters to measure air temperature, relative humidity, wind speed, precipitation and barometric pressure at 10-minute intervals.

2.2. Data preparation

2.2.1. The data

The data from the Rollesbroich station covered the period of six years from the 1st of January 2013 until 31st of December 2018. Variables were measured at different time resolutions and frequencies (Table 2). All the variables were transformed to daily values to ensure comparability of variables and accuracy of calculations. In addition, for relative humidity and air temperature, minimum and maximum daily values were used during the calculation of potential evapotranspiration (ET_0). Measured shortwave radiation was first converted to $J\ m^{-2}$ with subsequent conversion to the $MJ\ m^{-2}$. Finally, values of grass (dry) biomass measured on the 3-4 cuts per growing season were accumulated for subsequent comparison with simulations of harvested biomass in the model.

Table 2. Summary of the used data with conversion procedures.

Variable	Initial time resolution	Initial units	Converted daily units	Conversion method
Wind speed		$m\ s^{-1}$	$m\ s^{-1}$	average
Air temperature		$^{\circ}C$	$^{\circ}C$	mean
Relative humidity		%	%	-
Shortwave radiation	10 minutes	$W\ m^{-2}$	$MJ\ m^{-2}$	sum + unit
Rain gauge precipitation		mm	cm	sum + unit
Water contents		$cm^3\ cm^{-3}$	$cm^3\ cm^{-3}$	average
Pressure heads		hPa	hPa	average
Lysimeter precipitation		mm	cm	sum + unit
Lysimeter evapotranspiration	hourly	mm	cm	sum + unit
Percolation		mm	cm	sum + unit
Dry biomass	daily	$g\ m^{-2}$	$g\ cm^{-2}$	unit
Leaf area index		$m^2\ m^{-2}$	$cm^2\ cm^{-2}$	-

2.2.2. Estimation of missing values

To ensure a high quality of the observations, the lysimeter data was initially processed by manual and automated plausibility checks followed by Adaptive Window and Adaptive Threshold filtering (AWAT) to exclude noise in the lysimeter weight changes (Gebler *et al.* 2015). It was thereafter assumed that increases and decreases in lysimeter weight (measured at 1-minute intervals) are related to precipitation and actual evapotranspiration, respectively.

Measured precipitation and evapotranspiration for the three soil lysimeters at Rollesbroich (Ro-1, Ro-3, Ro-5) was not continuous, as it included periods with missing values. On the other hand, drainage measurements at the bottom boundary of soil lysimeters were continuous without missing values. Gap-filling for the observations of evapotranspiration was not performed since the model filled the linearly interpolated values in the gaps during calibration and actual evapotranspiration was not used as a driving data in the model.

In order to estimate missing values in precipitation data from the lysimeter, a simple linear regression was performed between on-site rain gauge data (as the independent variable) and precipitation data measured for each lysimeter as the dependent variable. Subsequently, precipitation values approximated by this linear model were used to fill the missing data in precipitation data from soil lysimeters (Figure 5).
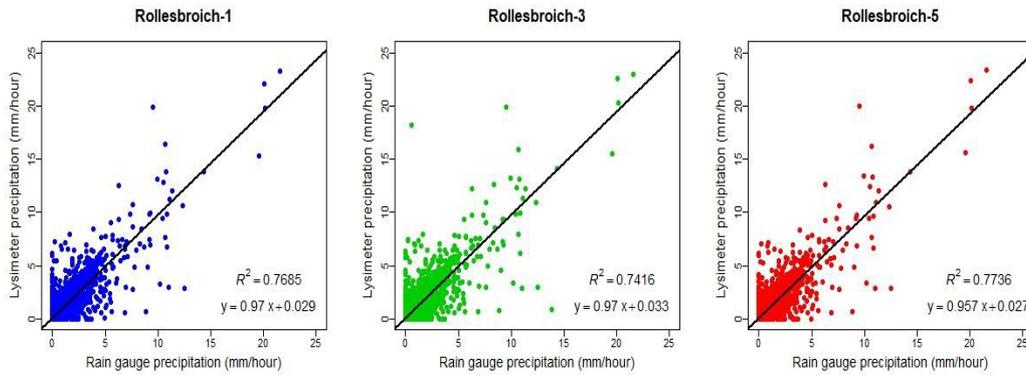
Figure 5. Linear models illustrating relationship of precipitation measured by lysimeters (Ro-1, Ro-3, Ro-5) versus rain gauge precipitation.

2.2.3. Potential Evapotranspiration (ET$_0$)

To calculate potential evapotranspiration (ET$_0$), the FAO Penman-Monteith equation was used as it has been shown to give the smallest errors in the estimation of potential evapotranspiration compared to other available methods in humid climates (Allen *et al.* 1998). ET$_0$ was calculated following the steps from Allen *et al.* (1998) as:

$$ET_0 = \frac{0.408 \cdot \Delta \cdot (R_n - G) + \gamma \cdot \frac{900}{T+273} \cdot u_2 \cdot (e_s - e_a)}{\Delta + \gamma \cdot (1 + 0.34 \cdot u_2)} \qquad (2.1)$$

where ET$_0$ is the reference evapotranspiration [mm day^{-1}], Δ is the slope of vapour pressure vs. temperature curve [kPa °C^{-1}], R_n is the net radiation at the crop surface [MJ m^{-2} day^{-1}], G is the soil heat flux density [MJ m^{-2} day^{-1}], T is average daily temperature at height of 2 m [°C], γ is the psychometric constant [kPa °C^{-1}], u_2 is

the wind speed at 2 m height [m s^{-1}], e_s is the mean saturation vapour pressure [kPa], e_a is the actual vapour pressure [kPa]. As the soil heat flux (G) is small compared with net radiation (R_n), G was assumed negligible at a daily time scale and set to zero.

The derivation of the parameters needed to calculate ET$_0$ is presented in the following.

Average daily air temperature T [°C] was calculated by averaging the daily minimum (T_{min}) [°C] and maximum (T_{max}) [°C] temperatures:

$$T = \frac{T_{max} + T_{min}}{2} \tag{2.2}$$

Saturation vapour pressure, e° [kPa] at a given temperature T, is calculated from:

$$e°(T) = 0.6108 \cdot exp\left(\frac{17.27 + T}{T + 273.3}\right) \tag{2.3}$$

The mean saturation vapour pressure is therefore obtained by:

$$e_s = \frac{e°(T_{min}) + e°(T_{max})}{2} \tag{2.4}$$

Daily actual vapour pressure, e_a, is obtained from saturation vapour pressure at daily minimum and maximum temperature and measurements of daily minimum and maximum relative humidity:

$$e_a = \frac{e°(T_{min})\frac{RH_{max}}{100} + e°(T_{max})\frac{RH_{min}}{100}}{2} \tag{2.5}$$

where RH_{max} and RH_{min} are the daily maximum and minimum values of relative humidity [%] respectively.

The slope of the saturation vapour pressure vs. temperature curve Δ is calculated from mean air temperature as:

$$\Delta = \frac{4098 \cdot [0.6108 \cdot exp(\frac{17.27 \cdot T}{T + 237.3})]}{(T + 237.3)^2} \tag{2.6}$$

The relationship of the partial pressure of water vapour to the air temperature, which denotes the psychrometric constant γ, depends on the atmospheric pressure, P [kPa]:

$$\gamma = \frac{c_p \cdot P}{\varepsilon \cdot \lambda} = 0.665 \cdot 10^{-3} \cdot P \tag{2.7}$$

where γ is psychrometric constant [kPa °C], c_p is specific heat at constant pressure ($c_p = 1.013$) [kPa °C], ε is the ratio of the molecular weight of water vapour and air ($\varepsilon = 0.622$) and λ is latent heat of vaporization ($\lambda = 2.45$) [MJ kg^{-1}]. Due to the small

influence of atmospheric pressure on ET_0, an average value of P for Rollesbroich is calculated based on the site elevation:

$$P = 101.3 \cdot \left(\frac{293 - 0.0065 \cdot z}{293}\right)^{5.26} \tag{2.8}$$

where P is atmospheric pressure [kPa] and z is the elevation of the location above sea level (511 m).

The difference between incoming net shortwave radiation (R_{ns}) and outgoing net longwave radiation (R_{nl}) denotes the net radiation (R_n):

$$R_n = R_{ns} - R_{nl} \tag{2.9}$$

The balance between incoming and reflected solar radiation results in net shortwave radiation, R_{ns} [MJ m^{-2} day^{-1}]:

$$R_{ns} = (1 - \alpha) \cdot R_s \tag{2.10}$$

where α is the albedo (the reflection coefficient of the canopy which is given a typical value of 0.23 [-]) and R_s is the incoming solar radiation [MJ m^{-2} day^{-1}].

Net longwave radiation R_{nl} [MJ m^{-2} day^{-1}] was estimated with the empirical equation suggested by FAO:

$$R_{nl} = \sigma \left[\frac{T_{max,K}^4 + T_{min,K}^4}{2}\right] \cdot (0.34 - 0.14 \cdot \sqrt{e_a}) \cdot \left(1.35 \cdot \frac{R_s}{R_{so}} - 0.35\right) \tag{2.11}$$

where , σ is the Stefan-Boltzmann constant [MJ m^{-2} K^{-4} day^{-1}], T_{max} is the maximum absolute daily temperature [K = °C+273.16], T_{min} is the minimum absolute daily temperature [K = °C+273.16] and R_{so} is the clear-sky (i.e. maximum possible) incoming shortwave radiation [MJ m^{-2} day^{-1}]. Calculation of other parameters (clear-sky radiation, extra-terrestrial radiation, inverse relative distance Earth-Sun, solar declination and sunset hour angle) which were needed to estimate net longwave radiation (R_{nl}) are listed in Appendix A (equations A1-A5).

2.3. Model description

2.3.1. Richards' equation

Combining the continuity and Darcy-Buckingham equations results in Richards' equation, which was used to describe water flow in unsaturated soil (Richards, 1931).

$$\frac{d\theta}{dt} = \frac{d}{dz}\left(K(\theta)\frac{dh}{dz} + 1\right) - U \tag{2.12}$$

where t is time (h), θ is volumetric water content [cm^{-3} cm^{-3}], z is height [cm], $K(\theta)$ is unsaturated hydraulic conductivity [cm h^{-1}], h is pressure head [cm] and U is a sink term to account for water uptake by plant roots.

In order to apply Richards' equation in the numerical model used in this study, both the continuity and Darcy-Buckingham equations were written in "finite form". The continuity equation in discrete form, which was used in model, is written as:

$$\frac{\Delta\theta}{\Delta t} = -\frac{\Delta q}{\Delta z} = -\frac{q_{z+\Delta z} - q_z}{\Delta z} \tag{2.13}$$

where Δt is the time step, $\Delta\theta$ is the change in water content during Δt, Δz is the vertical distance across which the water flow occurs, Δq is the difference in the water flow rates entering and leaving the soil layer, q_z is the water flow across the lower boundary of layer and $q_{z+\Delta z}$ is flow across the upper boundary of the soil layer, both given by the Darcy-Buckingham equation in discrete form:

$$q_{z+\Delta z} = -K\left(\frac{h_{i+1} - h_i}{\Delta z} + 1\right) \tag{2.14}$$

$$q_z = -K\left(\frac{h_i - h_{i-1}}{\Delta z} + 1\right) \tag{2.15}$$

where $i+1$ and $i-1$ denote pressure head values in the layers above and below layer i while K is the average hydraulic conductivity of the neighbouring two layers. The first term in brackets denotes the capillary gradient driving water flow while the second denotes the additional driving force of gravity.

2.3.2. Soil hydraulic properties

The water retention curve denotes the relationship between water content θ [cm^3 cm^{-3}] and soil water potential (h) [cm]. Due to its simplicity and fitting ability, the

van Genuchten (1980) equation for water retention has gained high popularity in scientific research:

$$\theta(\psi) = \theta_r + \frac{\theta_s - \theta_r}{[1+(\alpha|\psi|)^n]^{1-1/n}} \tag{2.16}$$

where θ_r is the residual water content [cm^3 cm^{-3}], θ_s is the saturated water content [cm^3 cm^{-3}], α is the inverse of the air entry suction [1/m] and n is the pore size distribution index [-].

Unsaturated hydraulic conductivity $K(\theta)$ is calculated using the Mualem model (van Genuchten, 1980) with the "matching point" K defined at a pressure head of 10 cm, as this gives a more reliable estimation of unsaturated hydraulic conductivity (K):

$$K(\theta) = K_{10}\left(\frac{S}{S_{10}}\right)^\tau \left[\frac{1-\left(1-S^{\frac{n}{n-1}}\right)^{(1-\frac{1}{n})}}{1-\left(1-S_{10}^{\frac{n}{n-1}}\right)^{(1-\frac{1}{n})}}\right]^2 \tag{2.17}$$

where K_{10} is the hydraulic conductivity at a pressure head of 10 cm, τ is the tortuosity [-] and the water saturation (S) and effective water saturation at a suction of 10 cm (S_{10}) were calculated assuming residual water content (θ_r) equals 0:

$$S = \frac{\theta}{\theta_s} \tag{2.18}$$

$$S_{10} = (1 + |10\alpha|^n)^{\frac{1}{n}-1} \tag{2.19}$$

A global pedotransfer function suggested by Jarvis *et al.* (2013) was used to derive hydraulic conductivity at a pressure head of -10 cm (K_{10}) from clay content:

$$K_{10} = 10^{A-B\cdot f_{clay}} \tag{2.20}$$

where A and B are empirical coefficients [-] and f_{clay} is the soil clay content [%].

2.3.3. Discretization, initial and boundary conditions

Based on the soil profile description every two horizons up to the depth of 140 cm were merged based on the assumption of similar textural class to ensure model simplicity and consistency with available input data. In order to maintain a constant layer thickness, 3 cm in total was cut off from the 2nd and 3rd horizons and 1 cm was added to the deepest horizon due to the odd layer thicknesses in the soil profile description. To ensure numerical stability of the model the merged soil profile was discretized into 23 numerical layers, each 6 cm in thickness (Figure 6). Finally, numerical values in the model were recalculated approximately every 11 minutes leading to 128 simulations per day in total.

The upper boundary condition in the model mimics the effect of precipitation so

the flow across the upper boundary is equal to the measured daily precipitation. The bottom boundary condition is defined by the earlier mentioned Darcy's law

(equation 2.15), with the only difference that the distance of water flow is equal to half of the layer thickness. The hydraulic gradient at the lower boundary of the soil profile is defined by the pressure head (h) measurements at a depth of 1.4 meters.
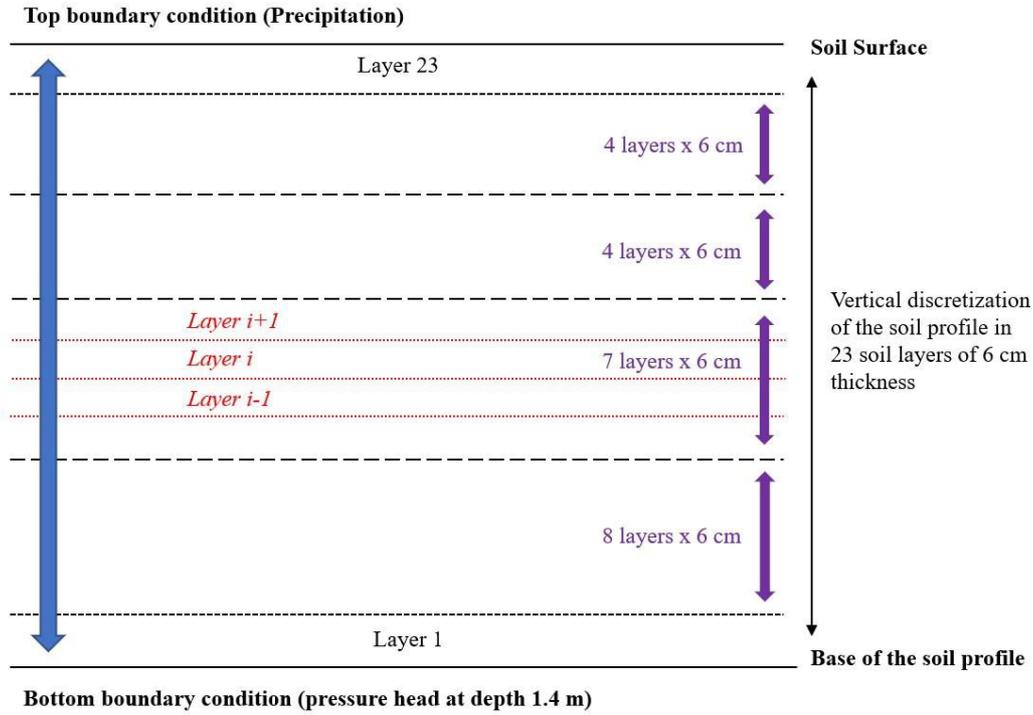
Figure 6. Schematic illustration of the discretized soil profile into 23 soil layers.

Initial water content (θ_i) in the hydrological model was approximated from initial pressure heads measured at 3 depths and van Genuchten model parameters:

$$\theta_i = (\theta_s(1 + |\alpha \cdot h_i|^n)^{(\frac{1}{n} - 1)}) \tag{2.21}$$

2.3.4. Plant water uptake

An empirical root water uptake model proposed by Jarvis (1989) was used to calculate water uptake sink in each soil layer, (U), yielding total transpiration rate as a sum of sink terms of all layers. It is relatively simple and parsimonious plant water uptake model accounting for compensatory water uptake that does not demand too many input parameters describing soil-root-water interactions. The actual transpiration (ET_a) [cm day^{-1}] simulated by the model is given by a function of the potential transpiration rate (ET_0) [cm day^{-1}] and a water stress index which reflects the plant response to drought conditions, varying between 0 (no transpiration) and 1 ($ET_a = ET_0$). The critical water stress index (ω_c) varying

between zero and one corresponds to a threshold value of the water stress index (ω) at which ET_a becomes smaller than ET_0:

$$ET_a = ET_0 \left(min \left(1, \frac{\omega}{\omega_c}\right)\right) ; \omega \leq \omega_c$$

$$(2.22)$$

$$ET_a = ET_0 \qquad\qquad ; \omega > \omega_c$$

The smaller the value of ω_c, the greater the degree of uptake compensation. The water stress index is given by the product of root allocation ($R_{z(i)}$) in each soil layer and an empirical parameter reflecting local resistance to water flow towards the roots (α_i):

$$\omega = \Sigma_{i=}^{i=n} R_{z(i)} \alpha_i \qquad\qquad\qquad (2.23)$$

where n is the number of soil layers in the profile.

The local soil resistance term (α_i) is expressed as a threshold function of the degree of saturation (S_i) in each soil layer:

$$\alpha_i = \frac{S_i - S_{w(i)}}{S_{c(i)} - S_{w(i)}} ; S_i < S_{c(i)}$$

$$(2.24)$$

$$\alpha_i = 1 \qquad\qquad ; S_i \geq S_{c(i)}$$

where $S_{w(i)}$ is the degree of saturation at permanent wilting point and $S_{c(i)}$ is the critical degree of saturation at reduced local uptake.

A critical degree of saturation ($S_{c(i)}$) is calculated under the assumption that it is reached when a given fraction (C_d) of the available water remains in the soil layer:

$$S_{c(i)} = C_d \cdot (1 - S_{w(i)}) + S_{w(i)} \qquad\qquad (2.25)$$

Vertical root distribution in the model was calculated based on the asymptotic equation proposed by Gale and Grigal, (1987) seen in equation 2.26.

$$Y = 1 - \beta^d \qquad\qquad\qquad (2.26)$$

Y is accumulated root biomass [varying from 0 to 1] from the surface to the depth of interest d [cm] and β is an estimated empirical parameter which is <1. As noted by Jackson *et al.* (1996), at high β values root proportion is greater in deeper soil horizons and greater proportion of the roots near the soil surface is at low β values. The proportion of root biomass, $R_{z(i)}$ in each soil layer (i) was calculated as (Bai *et*

al. 2017):

$$R_{z(i)} = \beta^{d^{(i-1)}} - \beta^{d^{(i)}} \tag{2.27}$$

where $d^{(i-1)}$ and $d^{(i)}$ are depths of the bottom and upper boundary of the soil layer (i), respectively. In addition, for the top layer $d^{(i)} = 0$ and for the bottom layer $\beta^{d^{(i)}} = 0$. β values can be used to calculate a maximum root depth z_{max} [cm^{-1}] beyond which 99 % of plant roots are located:

$$z_{max} = \frac{-2}{log_{10}(\beta)} \tag{2.28}$$

The macroscopic "sink" (U_i) describing water uptake in each soil layer is calculated assuming that the actual transpiration is distributed among soil layers in proportion to the distribution of the stress index:

$$U_i = ET_a \left[\frac{\alpha_i R_{z(i)}}{\omega}\right] \tag{2.29}$$

2.3.5. Plant growth

A simple equation was introduced to account for the temporal change of above-ground plant biomass:

$$\frac{dC_{leaf}}{dt} = G_L - d_{leaf} C_{leaf} - H \tag{2.30}$$

where (G_L) is the daily leaf growth [g cm^2 d^{-1}], d_{leaf} is a decay coefficient [1/day], C_{leaf} is the above ground biomass [g cm^2] and H is the harvest of above-ground biomass.

Daily leaf growth (G_L) [g cm^2 d^{-1}] is calculated from water-use-efficiency (WUE) [g cm^{-3} H$_2$O], daily actual evapotranspiration (ET$_a$) [cm d^{-1}] and aboveground biomass fraction (ϕ_{AG}) [-] from:

$$G_L = WUE \cdot ET_a \cdot \phi_{AG} \tag{2.31}$$

Harvest of above-ground biomass is controlled by binary variable (H_t) indicating the known occurence (= 1) or absence (= 0) of harvest on the day:

$$H = \frac{H_t \cdot C_{leaf}}{\Delta t} \tag{2.32}$$

2.4. Parameter estimation

2.4.1. Water retention curve

Optimization of van Genuchten model parameters (θ_s, n and α) was performed using the generalized reduced gradient (GRG) method in Excel solver add-in by minimizing the value in the objective cell through variation of "dummy" data parameter values (θ_s, θ_r, n, α) under constraints mentioned in equations 2.34-2.36. Minimizing the sum of squared errors (SSE) was selected as the objective of the optimization. The SSE is a measure of the difference between observed and modelled water content values (Barati, 2013):

$$SSE = \sum_{k=1}^{N} (\theta(h_k)_r - \theta(h_k)_e)^2 \tag{2.33}$$

where $\theta(h_k)_r$ is the measured soil water content, $\theta(h_k)_e$ is the estimated water content value and N is the total number of measurements.

Subject to,

$$0.01 \leq \alpha \ [1/m] \tag{2.34}$$
$$1.01 \leq n \tag{2.35}$$
$$0 = \theta_r \tag{2.36}$$

Residual water content (θ_r) was set to zero to simplify the model. No constraint was imposed on the variation of saturated water content (θ_s). The objective function (SSE) indicates a better estimation when it approaches zero, since it is the measure of the difference between measured and modelled soil water contents.

The derived parameter values shown in Table 3 lie within the range found by other authors (Silva and Coelho, 2014). MVG model parameters show variation at each depth and between lysimeters implying spatial heterogeneity of soil physical and hydraulic properties.

Table 3. Estimated MVG soil retention curve parameters with lowest objective function value.

| Soil depth (cm)	Lysimeter	θ_s (cm³/cm³)	α (1/m)	n (-)	Objective function
10	Ro-1	45.1	2.24	1.17	1689
	Ro-3	48.5	8.25	1.12	511
	Ro-5	48.4	3.23	1.19	1878
30	Ro-1	40.3	2.32	1.08	687
	Ro-3	40.9	2.84	1.08	684
	Ro-5	39.9	2.88	1.08	480
50	Ro-1	40.9	5.28	1.06	444
	Ro-3	40.5	5.07	1.07	225
	Ro-5	36.6	12.99	1.04	251

Figure 7 illustrates high R^2 values implying good explanation of variance of the dependent variable (pressure head) by the independent variable (water content).
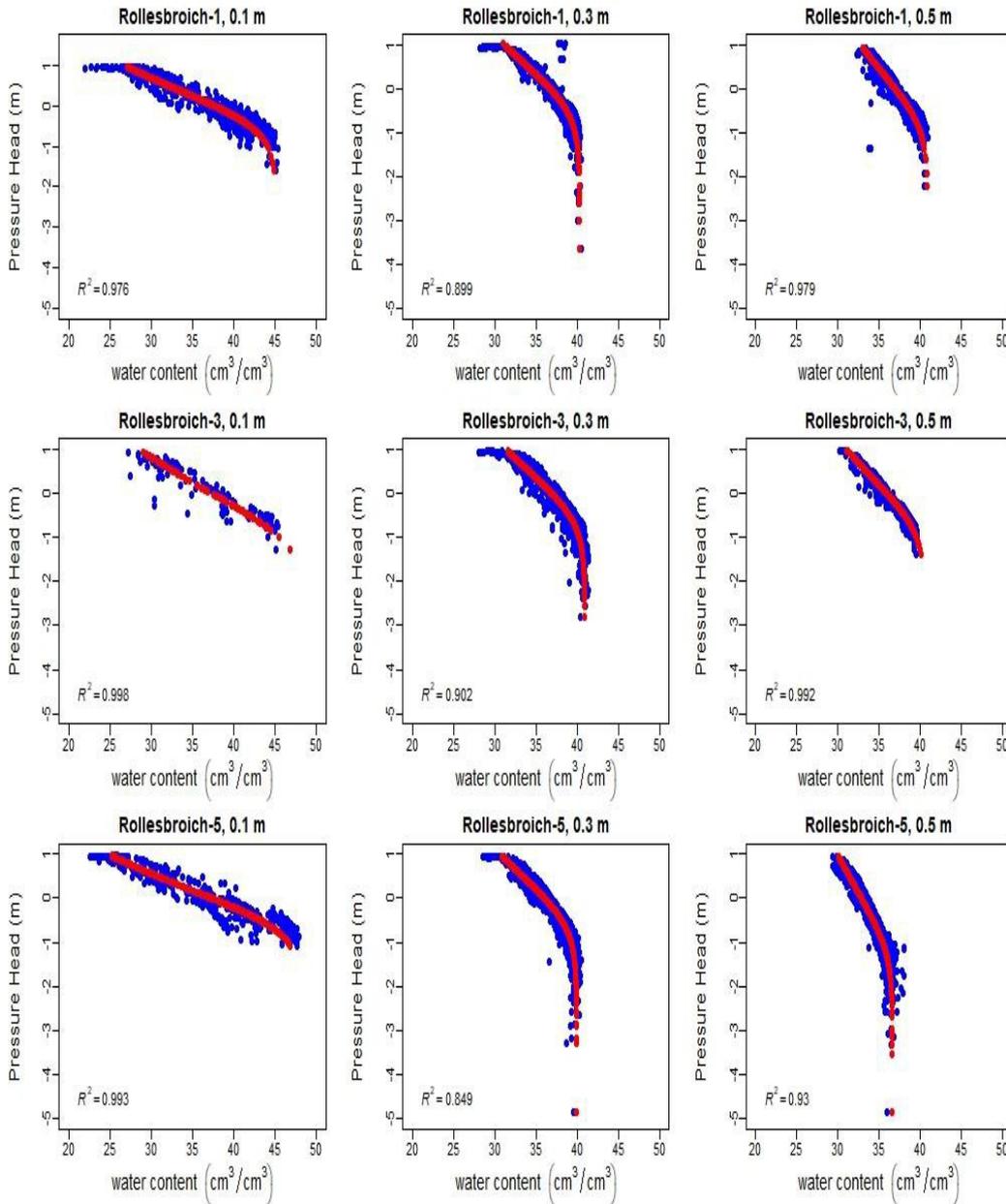
Figure 7. Best-fit MVG water retention curve with optimized model parameters (blue=observed values, red=modelled values).

The absence of soil water content and pressure head measurements at a depth below 0.5 meters in the lysimeters ruled out the possibility to estimate MVG model parameters for the deeper subsoil. The MVG model parameters measured at a depth of 0.1 meters were applied to depths greater than 0.5 m, since the textural class was similar.

2.4.2. Specific leaf area (SLA)

Leaf area index (LAI) [cm^2 cm^{-2}] was calculated from specific leaf area (SLA) [cm^2 g^{-1}] and initial aboveground biomass (C_{leaf}) [g cm^{-2}] seen in equation 2.37 (Sawada and Toshio, 2014).

$$LAI = SLA \cdot C_{leaf} \tag{2.37}$$

where average SLA was obtained from linear function with an intercept set to 0 by performing correlation between dry biomass (predictor) and LAI (predictand) values measured during the same time period (Figure 8).
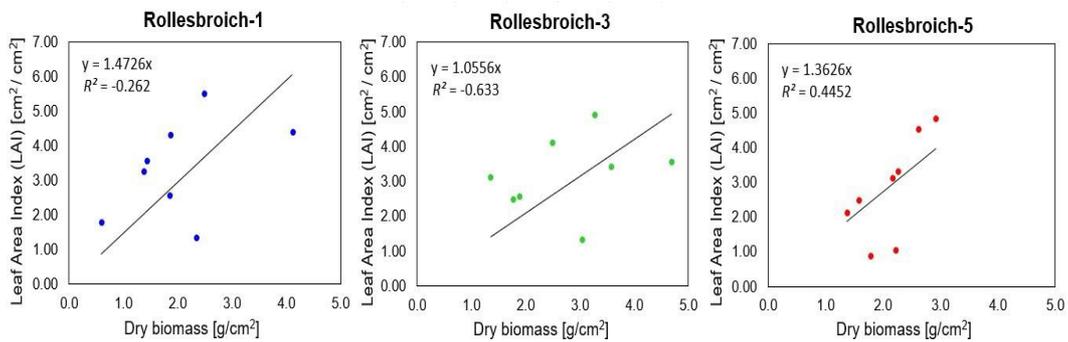

Figure 8. Estimation of SLA with infinite slope of linear regression between dry biomass and LAI for each soil lysimeter (Ro-1, Ro-3, Ro-5).

2.5. Model calibration and statistical analysis

2.5.1. Powell's method

Calibration can be defined as a technique which is used to find permissible parameter values describing a physical model with the best match to observed reality since all models are only approximations of nature (Gupta, Beven and Wagener, 2005).

Powell's method is one of the local optimization algorithms in unconstrained nonlinear optimization proposed by Powell, (1964) which estimates a local minimum n times through a linear search of the two-order function (Kobayashi and Maruyama, 1976):

$$f(x) = \frac{1}{2}x^T Ax + b^T x + c \tag{2.38}$$

where x is the vector of n variable, x^T is the transpose of vector x, A is the positive symmetric matrix, b is the parameter of vector and c is the parameter value.

A short description of the search of local minimum by Powell's method used in this paper is given in Appendix B (equations A6-A10). The algorithm is searching discrete space for the best set of parameter values locally and may converge at a set of parameter values which would not give the best model output in the case of several local maxima (Goffe, Ferrier and Rogers, 1994). Thus, it is important to set the maximum possible number of additional starts to avoid missing the best set of parameter values during the calibration procedure. During each start, the algorithm randomly chooses starting values of calibrated parameters from uniform distributions within an adopted range. As the optimum value search during each restart is carried out through many time-consuming simulations, calibration of each soil lysimeter in the STELLA software was performed 5 times with different initial guesses for five parameters, assuming the following ranges, within which the optimized parameters were assumed to be found:

$\cdot$ water $-$ use $-$ efficiency (WUE) $[g\ cm^{-3}\ H_2O] = 0.001 - 0.2$

$\cdot$ tortuosity (τ) $[cm\ cm^{-1}] = 0.01 - 0.99$

$\cdot$ critical deficit (C_d) $[-] = 0.01 - 0.99$

$\cdot$ critical stress index (ω_c) $[-] = 0.01 - 0.99$

$\cdot$ root distribution coefficient (β) $[-] = 0.914 - 0.972$

In order to evaluate the role of compensatory water uptake, additional calibration for Ro-1 lysimeter was performed with the critical stress index set to a constant value ($\omega_c = 1$) and excluded from the calibration procedure.

2.5.2. Goodness-of-fit

To evaluate the performance of the model, three statistical measures were calculated, the coefficient of determination (R^2), the mean absolute error (MAE) and the root mean squared error (RMSE):

$$R^2 = 1 - \frac{\sum_{i=1}^{n}(y_i - \hat{y}_i)^2}{\sum_{i=1}^{n}(y_i - \bar{y})^2} \tag{2.39}$$

$$MAE = \frac{1}{n} \cdot \sum_{i=1}^{n}|(y_i - \hat{y}_i)| \tag{2.40}$$

$$RMSE = \sqrt{\frac{1}{n} \cdot \sum_{i=1}^{n}(y_i - \hat{y}_i)^2} \tag{2.41}$$

where i is the control variable, n is the sample size, y_i stands for the measured values, $\hat{y}$ stands for the simulated values and $\bar{y}$ is the mean of measured values.

R^2 varies between zero and one with values of R^2 equal to one indicating that modelled values perfectly explain variation in observed values and R^2 value equal to zero meaning that modelled values failed to explain any of the variation in observed values (Miles, 2014). In other, words, a horizontal line through the mean of measured values on the y-axis explains these values better than modelled values on the x-axis.

It is not appropriate to use R^2 as the only parameter of the model fit since high R^2 values stating that modelled values almost perfectly explain variation in observed values, does not mean that model fit is good and goodness-of-fit could be obtained at low R^2 values since R^2 is unable to assess whether estimated coefficients and model predictions are biased (Armstrong, 2019).

Thus, two additional parameters of model fit, RMSE and MAE were applied which vary between zero and positive infinity indicating a good model fit at values close to zero.

3. Results

3.1. Model outcome

The best model fit during calibration with Powell's conjugate direction method was obtained with the set of parameters shown in Table 4. Parameter values do not differ so much between lysimeters except for critical deficit (C_d) which is much lower for lysimeter Ro-3 and uncompensated Ro-1 (NC) compared to other lysimeters. In addition, critical stress (ω_c) for lysimeter Ro-5 is slightly higher compared to other lysimeters.

Table 4. Best set of calibrated parameters for soil lysimeters with adopted range during calibration.

Parameter	Ro-1	Ro-1 (NC)	Ro-3	Ro-5	Sampled range
WUE	0.0066	0.0063	0.0083	0.0080	0.001- 0.2
τ	0.0100	0.0100	0.0554	0.0100	0.01 - 0.99
β	0.9574	0.9586	0.9589	0.9574	0.914 - 0.972
C_d	0.9854	0.4178	0.6854	0.9461	0.01 - 0.99
ω_c	0.4290	-	0.4532	0.5359	0.01- 0.99

3.1.1. Numerical analysis of the model results

Tables 5, 6 and 7 show calculated R^2, MAE and RMSE values to illustrate the goodness-of-fit of modelled results to observations of soil water contents, tensions, actual transpiration, percolation, harvested biomass and leaf area index. Tensions at all depths show slightly worse results compared to water contents with lower R^2 and higher MAE and RMSE values. Performance of the uncompensated model Ro-1 (NC) showed slightly better results compared to the Ro-1 model taking into account compensatory root water uptake.

Considering R^2, MAE and RMSE, the model gave the best results for lysimeter Ro-1 compared to the other two soil lysimeters (Tables 5 – 7). This may partly reflect the heterogeneity of soil properties, presence of larger gaps and outliers in the measurements of other lysimeters (Ro-3, Ro-5).

Table 5. Statistical output of model fit to observed data for Rollesbroich-1.

Variable	R^2		MAE		RMSE	
	Ro-1	Ro-1 (NC)	Ro-1	Ro-1 (NC)	Ro-1	Ro-1 (NC)
Water content, 0.1 m [cm^3 cm^{-3}]	0.881	0.871	0.027	0.028	0.033	0.035
Water content, 0.3 m [cm^3 cm^{-3}]	0.914	0.902	0.010	0.010	0.013	0.013
Water content, 0.5 m [cm^3 cm^{-3}]	0.929	0.922	0.008	0.008	0.010	0.010
logTensions, 0.1 m [hPa]	0.783	0.783	0.205	0.206	0.266	0.269
logTensions, 0.3 m [hPa]	0.744	0.742	0.249	0.247	0.358	0.357
logTensions, 0.5 m [hPa]	0.855	0.857	0.172	0.166	0.241	0.234
Actual evapotranspiration [cm day^{-1}]	0.839	0.844	0.049	0.049	0.067	0.067
Cum. actual evapotranspiration [cm]	1.000	1.000	2.472	3.269	2.937	3.763
Cum. percolation [cm]	0.998	0.998	3.046	3.148	3.776	3.744
ac. Harvest [g cm^{-2}]	0.987	0.987	0.023	0.015	0.028	0.018
Leaf area index (LAI) [cm^2 cm^{-2}]	0.563	0.567	0.869	0.834	1.027	0.985

Table 6. Statistical output of model fit to observed data for Rollesbroich-3.

Variable	R^2	MAE	RMSE
Water content, 0.1 m [cm^3 cm^{-3}]	0.787	0.041	0.051
Water content, 0.3 m [cm^3 cm^{-3}]	0.917	0.011	0.014
Water content, 0.5 m [cm^3 cm^{-3}]	0.944	0.009	0.012
logTension, 0.1 m [hPa]	0.750	0.197	0.264
logTension, 0.3 m [hPa]	0.753	0.260	0.371
logTension, 0.5 m [hPa]	0.846	0.159	0.216
Actual evapotranspiration [cm day^{-1}]	0.820	0.049	0.068
Cum. actual evapotranspiration [cm]	1.000	4.103	5.053
Cum. percolation [cm]	0.998	5.296	6.375
ac. Harvest [g cm^{-2}]	0.991	0.021	0.028
Leaf area index (LAI) [cm^2 cm^{-2}]	0.520	0.738	0.945

Table 7. Statistical output of model fit to observed data for Rollesbroich-5.

Variable	R^2	MAE	RMSE
Water content, 0.1 m [cm^3 cm^{-3}]	0.833	0.038	0.048
Water content, 0.3 m [cm^3 cm^{-3}]	0.909	0.010	0.013
Water content, 0.5 m [cm^3 cm^{-3}]	0.911	0.008	0.010
logTension, 0.1 m [hPa]	0.770	0.230	0.292
logTension, 0.3 m [hPa]	0.749	0.295	0.427
logTension, 0.5 m [hPa]	0.771	0.352	0.505
Actual evapotranspiration [cm day^{-1}]	0.800	0.053	0.072
Cum. actual evapotranspiration [cm]	1.000	2.929	3.661
Cum. percolation [cm]	0.998	2.605	3.440
ac. Harvest [g cm^{-2}]	0.994	0.068	0.080
Leaf area index (LAI) [cm^2 cm^{-2}]	0.546	1.131	1.303

The results obtained from this numerical analysis give quantitative information on model performance. However, graphical evaluation of simulation results should also be considered to make more precise statements about the model match to observed values.

3.1.2. Graphical analysis of the model results

In addition to numerical analysis, best-model-fits can be assessed through visual assessment with graphical methods such as temporal plots of modelled versus observed data as well as graphical assessment of model residuals.

Simulated and Observed Data over Time

Visual assessment of graphs illustrates a good fit of modelled water contents and tensions to observed data implying an acceptable model (Fig. 9-11). Most of the seasonal trends were well described by the model. As for the tensions, modelled results show small discrepancies at high tensions which, in addition to low number of observed points, could explain the slightly worse statistical results in comparison with water contents. In addition, tensiometers start to fail at high tensions (ca. 1000 hPa), so the model results are probably more reliable in estimation of these peaks.
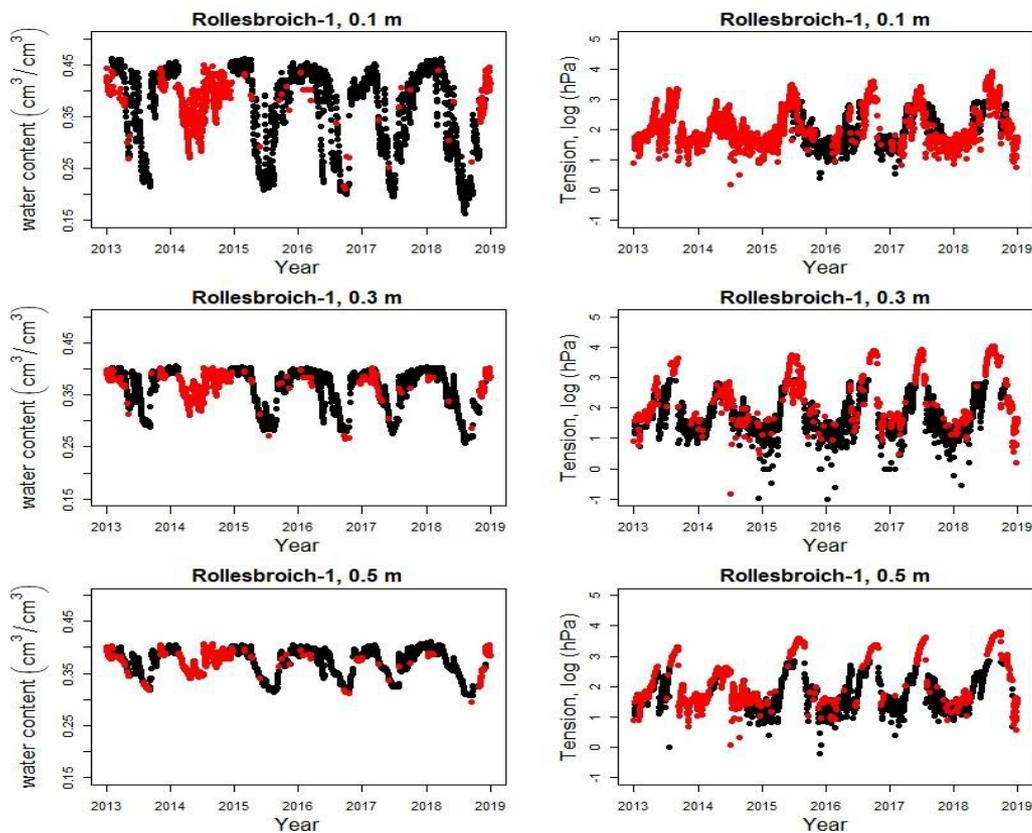

Figure 9. Water contents and tensions over time for Rollesbroich-1 (black=observed, red=modelled).
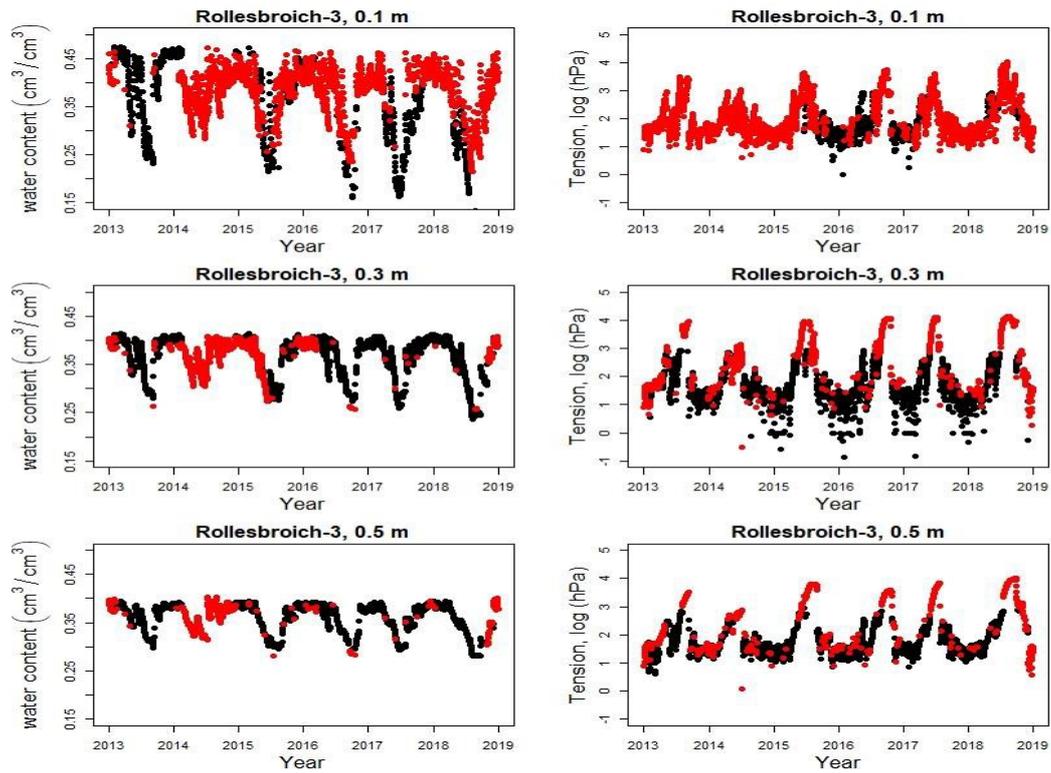
Figure 10. Water contents and tensions over time for Rollesbroich-3 (black=observed, red=modelled).
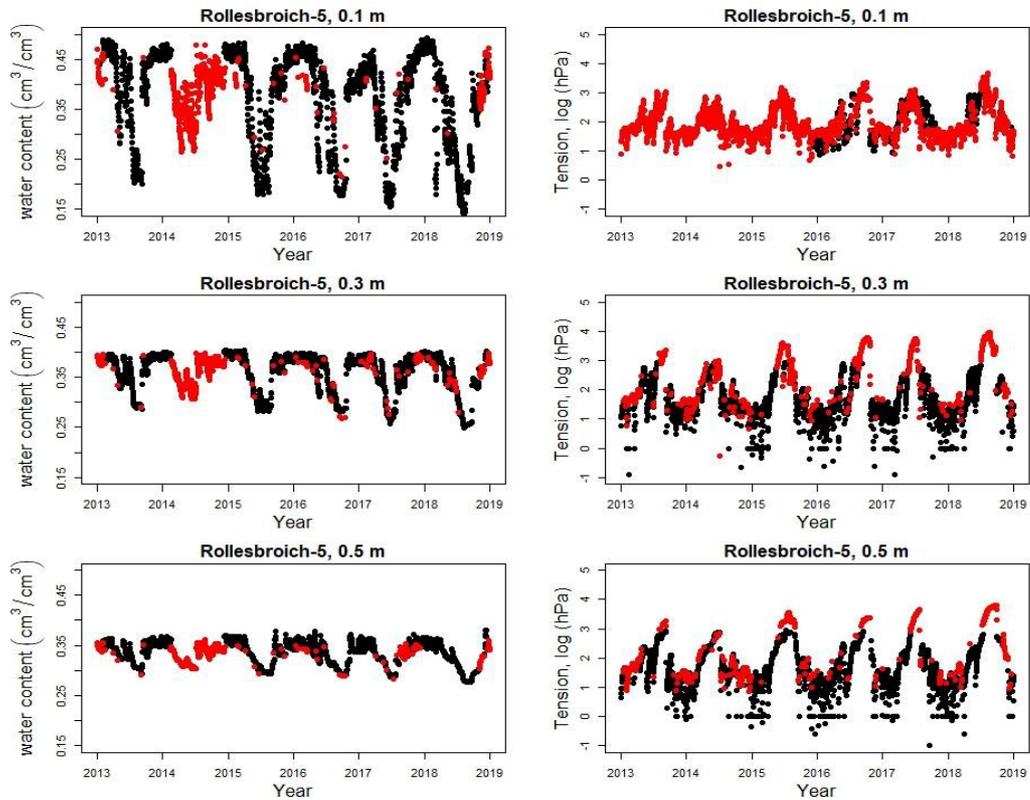

Figure 9. Water contents and tensions over time for Rollesbroich-1 (black=observed, red=modelled).

Modelled actual evapotranspiration shows an absence of outliers from potential evapotranspiration, with a good match to the falling and increasing rates observed during the winter and spring, respectively (Figure 12). Furthermore, the other modelled variables illustrate reasonable model fits to the observed data, except for accumulated harvest, which was overestimated by the model in Ro-5 (Figure 13). In addition, LAI also shows slightly higher values for Ro-5 compared to other soil lysimeters during the summer peaks, since it is related to the above-ground biomass.
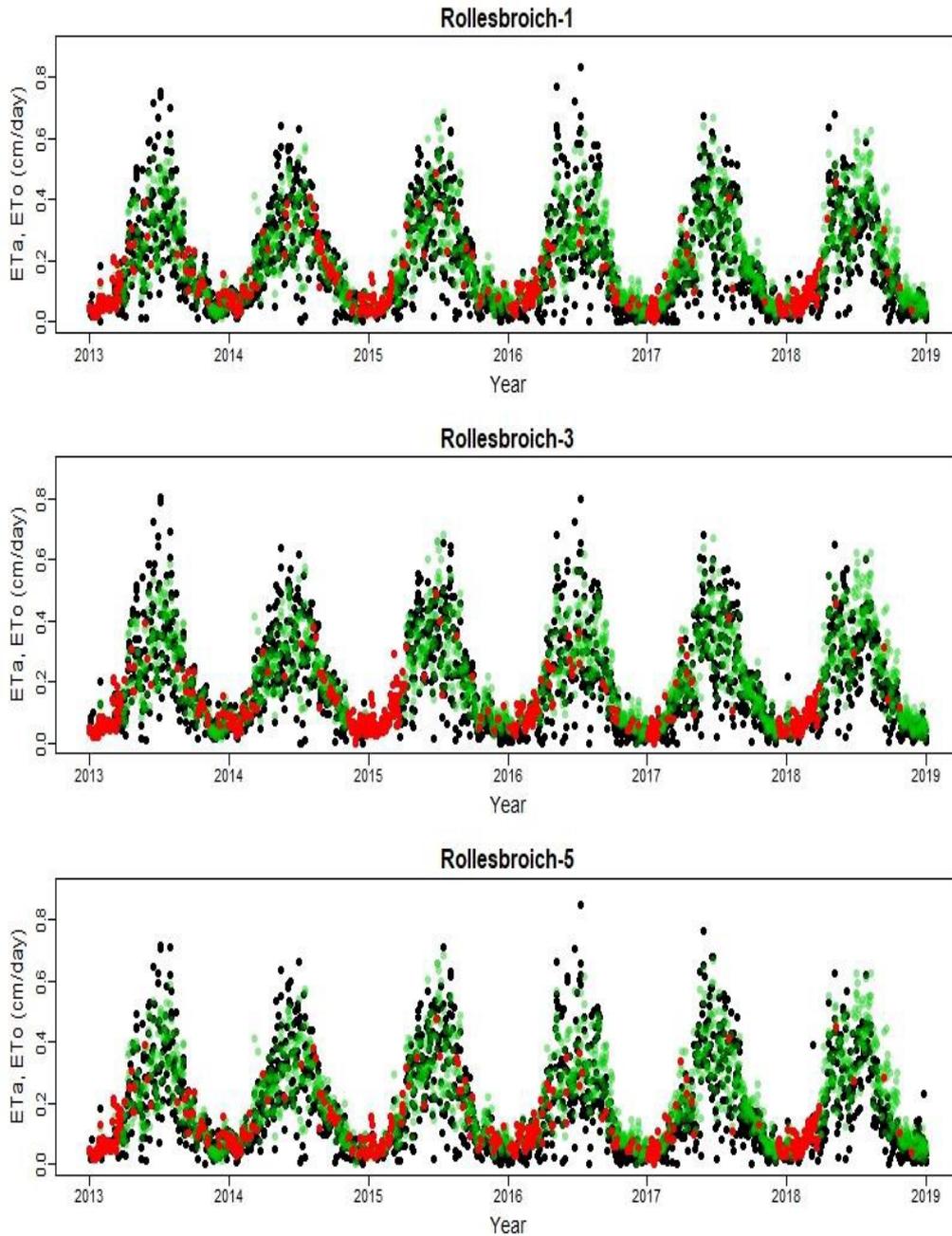

Figure 12. Time series of simulated (red) and observed (black) actual and potential (green) evapotranspiration for Rollesbroich lysimeters.
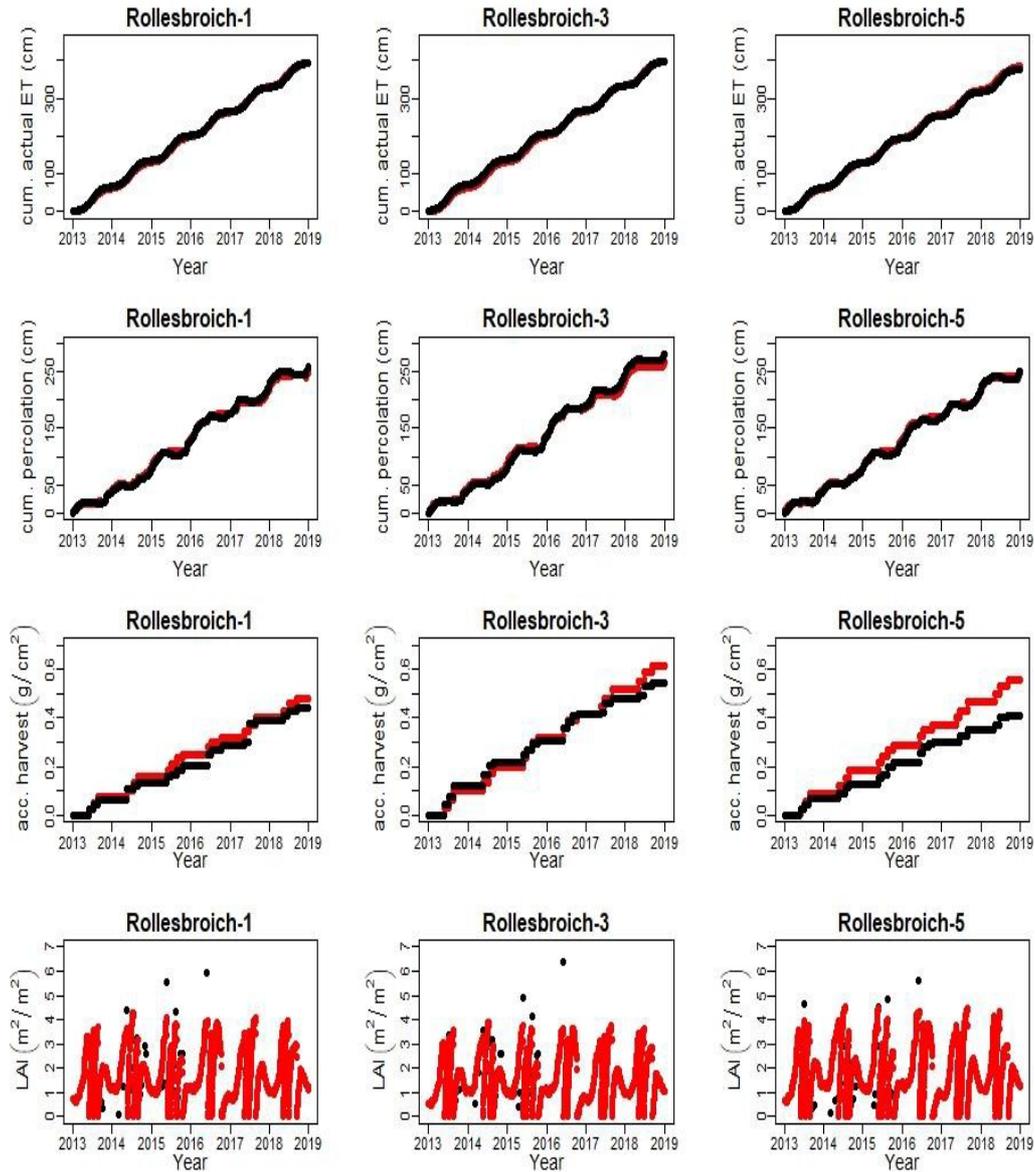
Figure 13. Leaf area index (LAI), cumulative percolation, harvest and evapotranspiration over time for all soil lysimeters (black=observed, red=modelled).

Residual Analysis

To further assess model performance, an analysis of residuals was performed. One of the methods of testing the goodness-of-fit of the model is to test for the equal variance of the model residuals, which is also called a test for homoscedasticity. In an ideal case, the standardized residuals should occupy equal space on the plot, exclude any asymmetry and in the case of clustering, residuals should cluster around low values of the y-axis and close to the middle of the plot (Rosopa, Schaffer and Schroeder, 2013).

In general, there are no clear signs of failing to meet the criteria for homoscedasticity for most of the variables excluding the minor case of outliers for all variables and visible trends at high tensions at depths of 0.1 and 0.3 m. For most variables, the residuals are randomly distributed and clustered across the lower values of the y-axis around the best line of fit (set to zero) in the middle of the plot. However, for cumulative variables such as cumulative actual transpiration and percolation, there are visible signs of heteroscedasticity implying non-linearity of these variables (Fig. 14). There are also clear signs of autocorrelation of residuals in these variables, which is not surprising since for cumulative variables each value is dependent on the preceding value.
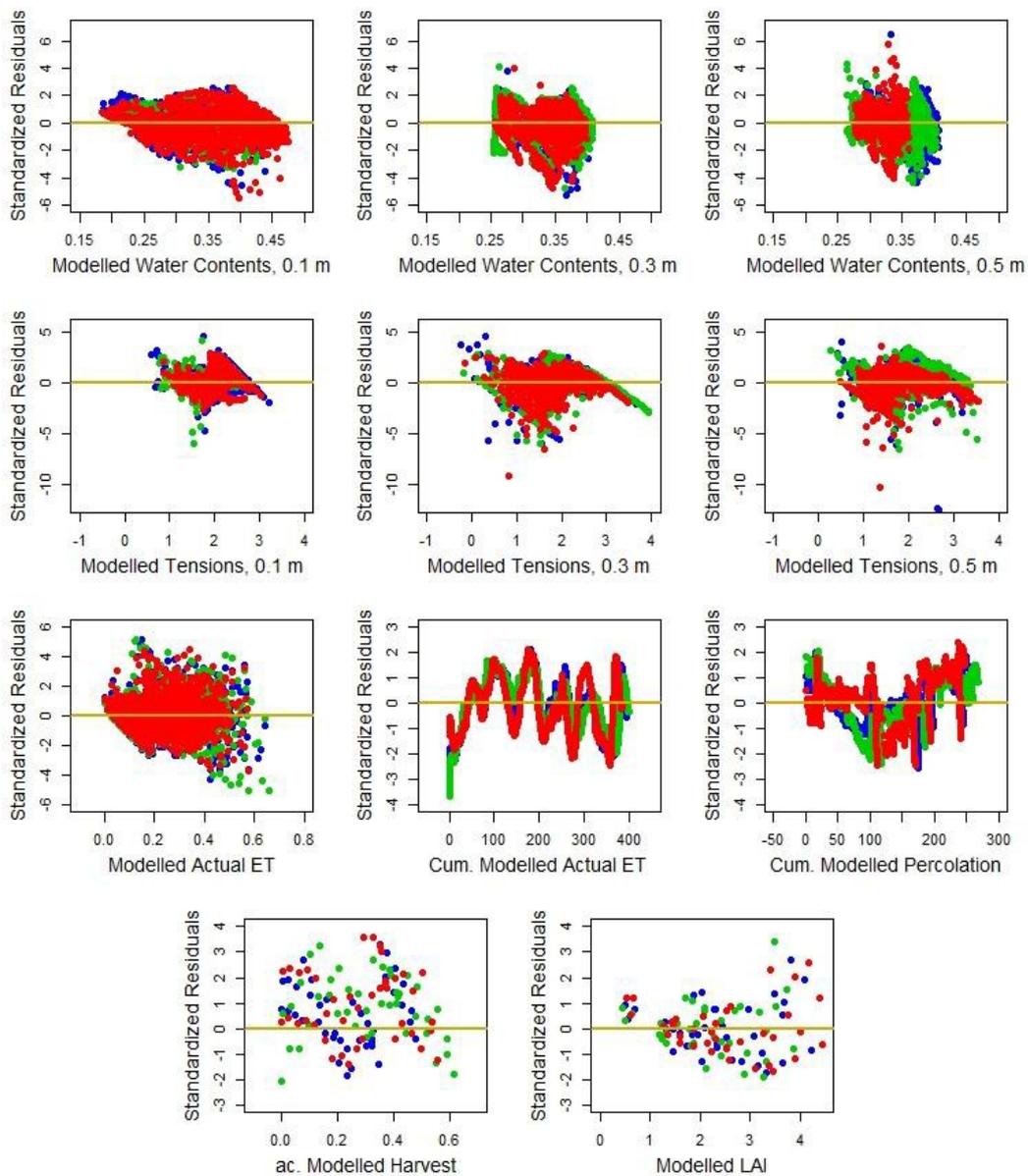

Figure 14. Standardized residual versus modelled values (blue=Rollesbroich-1, green=Rollesbroich-3, red=Rollesbroich-5).

Another common method to evaluate the goodness-of-fit is to check for a normal distribution of error terms (ε). This can be assessed through normal probability plots of residuals. To support the assumption of the normal distribution of the error terms, residuals should be located on the straight line (García Ben and Yohai, 2004).

According to Figure 15, out of all variables, tensions at a depth of 0.1 m and modelled LAI show signs of being normal distributions, if outliers are removed during data transformation. Water contents at depths of 0.1 and 0.3 m show signs of left-skewed data while accumulated harvest suffers from right skewness. Cumulative actual transpiration and percolation illustrate the presence of S-shaped curves with short tails, while distributions for all other variables have long tails.
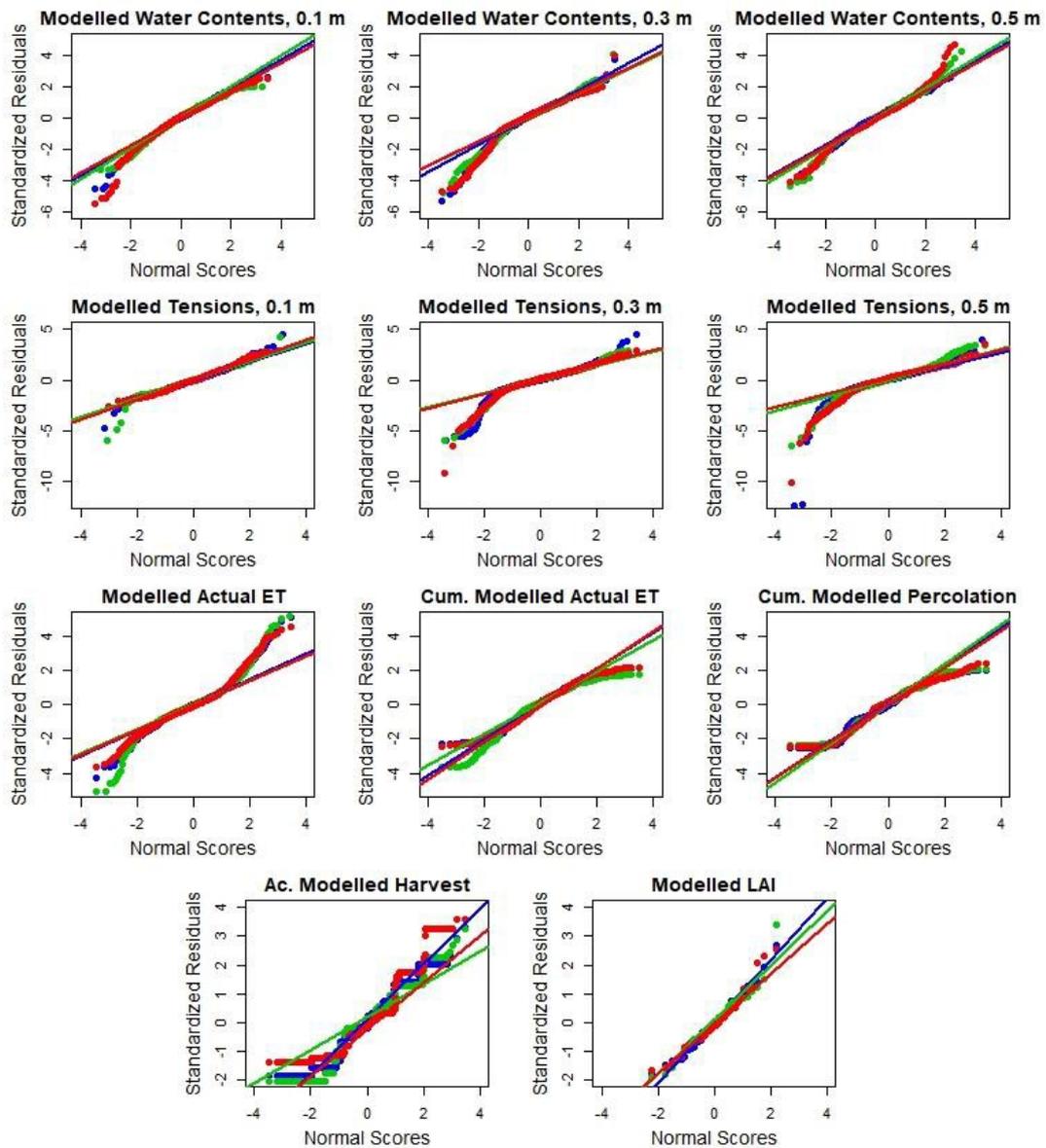

Figure 15. Normal probability plot of residuals (blue=Rollesbroich-1, green=Rollesbroich-3, red=Rollesbroich-5 with respective fit lines).

37

Methods trying to prove equality (Figure 14) and normal distributions (Figure 15) of residuals failed, although model fits were assessed as reasonable by numerical analysis. It can be concluded that a good model fit for the calibration period is not confirmed by the analysis of residuals. However, following Pallant (2007), a failure to meet the criterion of normal distributed residuals would not cause significant problems for large datasets with many observations (>30) and the normal distribution is important if parametric tests (ANOVA, t-test, etc.) are applied. In addition, potential cause of non-normal distribution of data could be the high resolution, extreme and near zero values and the different distribution of the modelled data (Weibull, log-normal, etc.) (Buthmann, 2016).

4. Discussion

4.1. Calibrated parameter values

The calibrated β values for the lysimeters were larger (0.9574-0.9589) than the average β value for the root distributions of temperate grasslands taken from a global database (Jackson *et al.* 1996), which was equal to 0.943, indicating a greater proportion of roots at depth. These β values show that up to the 99% of the plant roots are located above 106 cm for Ro-1 and Ro-5, while for Ro-3 the maximum plant root depth is equal to 110 cm. These values match well the initial soil profile description, which suggested that the maximum root depth is 127 cm, if we assume that only a few roots are reaching the observed depth. Such deep rooting may be explained by a low penetration resistance for plant roots (Gill, Sivasithamparam and Smettem, 2000), perhaps caused by the sandy loam texture and a lack of compaction throughout the soil profile due to the absence of traffic over the lysimeter. Albasha, Mailhol and Cheviron, (2015) state that compensatory water uptake is promoted by deeper rooting. Thus, obtained β values exceeding the values for the grassland from the global database during calibration implies the potential for compensatory root water uptake caused by deeper rooting profile. However, model calibration of the uncompensated model gave a maximum rooting depth of 109 cm, which is almost identical to the value obtained with the model which takes compensatory water uptake into account. A slightly better match of the uncompensated model to the data could be partly explained by the fact that the best set of the model parameters gained by the Ro-1 were used as initial starting values for Ro-1 (NC), so that finding the best set of model parameters was a bit easier for the optimization algorithm. On the other hand, graphical assessment of the model predictions for the gaps in observations as well as residual analysis were not performed leading to uncertainty as to which model gave a better performance.

Smaller tortuosity (τ) values obtained during calibration for Ro-1, Ro-1 (NC) and Ro-5 lysimeters compared to the slightly higher τ value for Ro-3 give a weaker decrease in soil hydraulic conductivity with a decrease in the soil water saturation (Cai *et al.* 2018). According to Schaap and Leij (2000), such small and even negative tortuosity values can be obtained for all textural groups, with the smallest values for clay and loam soils. It seems likely that negative values of tortuosity would have been obtained if this had been allowed by the parameter range, since optimized tortuosity values for Ro-1, Ro-1 (NC) and Ro-5 lysimeters were at the lower bound of the sampled range. Such physically unrealistic values imply that the physical conceptualization underlying Mualem's model (bundles of capillary tubes) is incorrect. It can be concluded that the tortuosity factor is in practice a complex factor of pore shape and connectivity and not just tortuosity.

The performed model optimization suggested the need for a compensatory water uptake mechanism since calibrated critical stress index values ($\omega_c < 1$) implied the presence of compensatory water uptake for all soil lysimeters. There are clear signs of decreasing transpiration rates relative to the potential transpiration rate under low soil pressure heads to a depth of 0.5 m, although compensatory water uptake was potentially relatively high (low ω_c). The value of the critical stress index (ω_c) depends on root and plant properties controlling potential evapotranspiration and a high potential for compensatory water uptake implies that the ratio of total root length to LAI is high (Jarvis, 2010; Jarvis, 2011).

According to Dos Santos *et al.* (2017), the model proposed by (Jarvis, 1989) was able to simulate cumulative actual transpiration more accurately than models not taking compensatory mechanism into account despite its low performance among compensatory uptake models. At high transpiration rates, applied model predicted higher and longer water uptake from the top layers leading to the faster soil water decrease in these layers and greater compensation of water from deeper layers while actual transpiration was close to potential evapotranspiration due to the low critical water stress index (ω_c) values. On the other hand, Dos Santos *et al.* (2017) found that the compensatory plant uptake model proposed by Jarvis (1989) is sensitive to the definition of local soil resistance term (α_i) leading to the potential reduction of α_i at near saturation values of the soil. Thus, the value of the water stress index (ω_c) which defines the compensatory water uptake by a plant depends on the definition of local soil resistance term (α_i). Lower critical deficit (C_d) value for the uncompensated model (Ro-1 (NC)) potentially contributed to the greater water uptake compared to the compensated model (Ro-1) with lack of compensation mechanism. Anyway, the data does not allow to distinguish between the two model since both models are calibrated well to the observations. This is a result of the wet climate conditions at the site leading to only shorter periods of stress throughout simulation.

4.2. Cause of model errors

Divergences between model predictions and observations can arise because of the errors caused by measurement devices, inappropriate parameter values or model limitations due to the wrong or insufficient mathematical descriptions of the complex behaviour of environmental processes.

The accumulated harvest from Ro-5 was overestimated despite the good match to this variable in the Ro-3 and Ro-1 lysimeters (Figure 13). A poor model performance in fitting to the accumulated harvest could potentially be explained by the influence of factors which were not considered in the model, such as plant diseases and other stress factors. The leaf decay coefficient value (d_{leaf}) was not included in the calibration process and a faster decay of above-ground biomass might have explained the smaller harvest. On the other hand, simulated evapotranspiration rates were similar to the other soil lysimeters, which is not consistent with evapotranspiration rates in the presence of some stress factors.

Following Allen *et al.* (1998) soil heat flux (*G*) was ignored in the calculation of potential evapotranspiration with FAO-56 Penman-Monteith equation, since at a given daily time step soil heat flux is small compared to the net radiation (R_n) and soil temperature might be assumed equal to air temperature. Despite the fact that the contribution of soil heat flux in the energy budget is less than 5% at a daily time step (Running and Kimball, 2005), for longer periods soil heat flux might be significant leading to underestimation of simulated evapotranspiration. In addition, a constant albedo (*α*) value of 0.23, which was used in the calculation of net shortwave radiation (R_{ns}) may not be realistic throughout the year in a given climate leading to potential bias in the calculation of net radiation (Xu *et al.* 2009).

Despite the fact that gap-filling procedure was not performed for evapotranspiration measurements from soil lysimeters, application of similar HYDRUS model (Šimůnek, van Genuchten and Sejna, 2011) which uses Richards' equation to simulate water flow in unsaturated zone gave a reliable estimation of missing evapotranspiration data for gaps of up to 30 days (Huang *et al.* 2020).

Leaf area index (LAI) was one of the error-prone variables in the soil-plant system since specific leaf area was estimated from a few data points of measured above-ground biomass and leaf area which were not always measured at the same time period leading to low R^2 values. A similar but less significant problem was experienced during gap-filling for climate data, since the more accurate precipitation data measured by lysimeter compared to the same dataset obtained by the rain gauge was used as a driving data in the model. Although R^2 values obtained by linear regression to fill the gaps in the precipitation data from the lysimeters were satisfactory they were still not outstanding which could lead to small errors potentially leading to direct and indirect effects on simulated soil water balance variables. Furthermore, as mentioned before, rain gauge measurements are also subject to various errors which leads to the necessity of precipitation correction in

meteorological studies (Ren and Li, 2007). However, in this study, the precipitation data measured by rain gauge was not corrected before gap-filling which could cause additional bias in values predicted by the linear regression model, especially considering the fact that during data preparation precipitation measurements were adjusted to cumulative daily values potentially causing high errors.

The pedotransfer function which was applied to estimate hydraulic conductivity (K_{10}) at a tension of 10 cm may introduce errors since it was calculated from a multivariate ordinary linear regression model (MLR) of a global database of tension infiltrometer data with only a modest performance in validation (Jarvis *et al.* 2013). In addition, in the scope of this project saturated matric hydraulic conductivity (K_{10}) was calculated based on the available clay content data while two other coefficients in the function related to bulk density and annual air temperature were assumed constant.

To avoid numerical errors, the soil profile was divided into sub-layers of constant thickness, which led to small errors in horizon thicknesses compared with the soil profile description. However, considering the fact that the soil profile description is also prone to human error and the commonly observed gradual changes between soil horizons, it was assumed that the resulting loss of soil horizon thickness (3 centimetres in total) would not cause significant deviations between model results and observations.

Powell's conjugate direction method, which was used to calibrate the set of model parameters may have not reached the global minimum in the discrete parameter space explored. The number of restarts was limited to five, due to the time required to calibrate such a complex numerical model, with the limited computational power of PC's. Thus, there is a possibility that the best set of calibrated model parameters was not found for this number of restarts.

4.3. Model limitations

Despite the weak performance of model results in residual analysis and slight deviations from observed values in simulated values during visual assessment of graphs, numerical analysis of the model output showed acceptable level of model performance for future applications. Unfortunately, time-constraints set some limitations on the scope of this paper, so the performance of potential model modifications such as alternative equations describing root growth and plant water uptake could not be considered in this thesis.

The Jarvis (1989) root water uptake model was applied here for a wet climatic region with only short periods of dryness, which prevented the model from demonstrating its main advantages to simulate compensatory water uptake from deeper soil layers under dry conditions. Anyway, for this dataset, the proposed root water uptake model was able to simulate observed trends in decreasing soil water content during dry periods, which could be related to potential compensatory water uptake of plant roots.

According to van Lier, Neto and Metselaar, (2009) pressure heads and hydraulic conductivity are independent soil variables in soil numerical models describing root water uptake. Thereby, a more complex fourth-order approximation of matric flux potential which denotes the combination of hydraulic conductivity (K) over the varying pressure head (h) values can be used to describe the water flow to plant roots with Richards equation in the unsaturated zone as one of the first model improvements. In addition, a recently proposed simple physics-based macroscopic model including a composite rooting parameter could be applied as an alternative model accounting for compensatory root water uptake in each soil horizon (van Lier *et al.* 2008; Jarvis, 2010). Furthermore, one of the shortcomings of the model used here was the absence of the control of root biomass on water uptake (Jarvis, 2010). Root biomass could be modelled considering root decay similarly to the decay of above-ground biomass (Ivanov, Bras and Vivoni, 2008). However, models are a simplified representation of reality, which should be kept in mind, as the model modifications mentioned above may increase uncertainty in simulated results. No model is capable of perfect explanations of the complex natural behaviour of water in the plant-soil-atmosphere continuum (Sánchez, 2006).

As reported by White and Chaubey, (2005) the standard procedure for numerical modelling should include sensitivity analysis, which is followed by calibration and model validation. In the scope of this project, a sensitivity analysis was not possible. Application of powerful sensitivity analysis methods such as Monte Carlo Simulation (MCS) to evaluate the influence of various model parameters on model outputs would give an idea of model parameters that should be included in the calibration and their ranges. This may have decreased the time required during calibration, since the adopted ranges of model parameters in the calibration procedure were set according to the literature.

Quality of the data which was used in this project permits to develop soil numerical models with a driving data at much finer scale than one day (10 minutes) to analyse complex interaction of plant-soil-atmosphere continuum with new research ideas.

5. Conclusions and recommendations

The main aim of this thesis was to test a numerical soil hydrological model using six years of measurements at a high time resolution of the soil water balance, soil water contents and tensions and grass growth in three lysimeters located in Rollesbroich, Germany. One of the aims was to highlight potential shortcomings of the model and suggest future improvements of the model.

Application of graphical and numerical analysis of model outputs to investigate the accuracy of the calibrated model showed that the numerical model was suitable to describe the complexity of the water flow processes in the plant-soil-atmosphere continuum. Numerical analysis of model outputs showed a good fit of simulated variables to observed data with R^2 values varying between 0.52 and 0.99, RMSE between 0.01 and 0.05 cm^3 cm^{-3} for water contents and 0.067 to 0.072 cm d^{-1} for actual evapotranspiration. On the other hand, even though visual assessment of model output suggested a good match to the main seasonal trends in the observations, analysis of the residuals showed a failure to meet the criterion of a normal distribution, which is one of the signs of a good model fit. However, given the large sample size of the variables, the results of this analysis of residuals were considered less significant.

The numerical model tested here is recommended as a basis for future studies of soil water balance under climate change. Given that the quality of the model fit varied with time as well as between replicate lysimeters, one of the suggestions would be to first carry out a sensitivity analysis as well as to increase the number of re-starts in the model calibration procedure, in order to investigate the uniqueness of the derived parameter values. Finally, it would be useful to simulate a dataset with measurements obtained under drier climate conditions, as this would represent a much more critical test of the performance of the compensatory water uptake model, especially in comparison with the uncompensated model. A test of these model variants using three Rollesbroich lysimeters which were re-allocated to Selhausen in a drier climate within the TERENO network is being planned for the near future, once the data becomes available.

References

Albasha, R., Mailhol, J. C. and Cheviron, B. (2015) 'Compensatory uptake functions in empirical macroscopic root water uptake models - Experimental and numerical analysis', *Agricultural Water Management*. doi: 10.1016/j.agwat.2015.03.010.

Alcamo, J., Moreno, J. M., Nováky, B., Bindi, M., Corobov, R., Devoy, R. J. N, Giannakopoulos, C., Martin, E., Olesen J. E. and Shvidenko, A. (2007) 'Europe. Climate Change 2007: Impacts, Adaptation and Vulnerability', *Contribution of Working Group II to the Fourth Assessment Report of the Intergovernmental Panel on Climate Change*, Eds., Cambridge University Press, Cambridge, UK, pp. 541-580. doi: 10.2134/jeq2008.0015br.

Allen, R. G., Pereira, L. S., Raes, D. and Smith, M. (1998) 'Crop evapotranspiration - guidelines for computing crop water requirements', FAO Irrigation and drainage paper 56, Food and Agriculture Organization, Rome.

Armstrong, R. A. (2019) 'Should Pearson's correlation coefficient be avoided? ', *Ophthalmic and Physiological Optics*. doi: 10.1111/opo.12636.

Bai, Y., Zhang, J., Zhang, S., Koju, U. A., Yao, F. and Igbawua, T. (2017) 'Using precipitation, vertical root distribution, and satellite-retrieved vegetation information to parameterize water stress in a Penman-Monteith approach to evapotranspiration modeling under Mediterranean climate', *Journal of Advances in Modeling Earth Systems*, 9(1). doi: 10.1002/2016MS000702.

Barati, R. (2013) 'Application of excel solver for parameter estimation of the nonlinear Muskingum models', *KSCE Journal of Civil Engineering*, 17(5), pp. 1139–1148. doi: 10.1007/s12205-013-0037-2.

Bogena, H., Kunkel, R., Pütz, T, Vereecken, H., Krüger, E., Zacharias, S., Dietrich, P., Wollschläger, U., Kunstmann, H., Papen, H., Schmid, H. P., Munch, J. C., Priesack, E., Schwank, M., Bens, O., Brauer, A., Borg, E. and Hajnsek, I. (2012) 'TERENO—Ein langfristiges Beobachtungsnetzwerk für die terrestrische Umweltforschung', (In German, with English abstract.) Hydrol. Wasserwirt. 53: pp. 138–143.

Boeck, H. J., Lemmens, C. M. H. M., Gielen, B., Bossuyt, H., Malchair, S., Carnol, M., Merckx, R., Ceulemans, R. and Nijs, I. (2007) 'Combined effects of climate warming and plant diversity loss on above- and below-ground grassland productivity', *Environmental and Experimental Botany*. doi: 10.1016/j.envexpbot.2006.07.001.

Boeck, H. J., Lemmens, C. M. H. M., Zavalloni, C., Gielen, B., H., Malchair, S., Carnol, M., Merckx, R., van den Berge, J., Ceulemans, R. and Nijs, I. (2008) 'Biomass production in experimental grasslands of different species richness during three years of climate warming', *Biogeosciences*. doi: 10.5194/bg-5-585-2008.

Buthmann, A. (2016) 'Dealing with Non-normal Data: Strategies and Tools', *iSixSigma*.

Cai, G., Vanderborght, J., Langensiepen, M., Schnepf, A., Hüging, H. and Vereecken, H. (2018) 'Root growth, water uptake, and sap flow of winter wheat in response to different soil water conditions', *Hydrology and Earth System Sciences*. doi: 10.5194/hess-22-2449-2018.

Chen, R. S., Pi, L. C. and Hsieh, C. C. (2005) 'Application of parameter optimization method for calibrating tank model', *Journal of the American Water Resources Association*. doi: 10.1111/j.1752-1688.2005.tb03743.x.

Condon, A. G., Richards, R. A., Rebetzke, G. J. and Farquhar, G. D. (2004) 'Breeding for high water-use efficiency', in *Journal of Experimental Botany*. doi: 10.1093/jxb/erh277.

Easterling, W. E., Aggarwal, P. K., Batima, P., Brander, K., Lin, E., Howden, S. M., Kirilenko, A. P., Morton, J., Sousanna, J. -F., Schmidhuber, J. and Tubiello, F. N. (2007) 'Food, fibre and forest products', in *Climate Change 2007: Impacts, Adaptation and Vulnerability. Contribution of Working Group II to the Fourth Assessment Report of the Intergovernmental Panel on Climate Change*.

Evett, S. R., Schwartz, R. C., Howell, T. A., Baumhardt, R. L. and Copeland, K. S. (2012) 'Can weighing lysimeter ET represent surrounding field ET well enough to test flux station measurements of daily and sub-daily ET?', *Advances in Water Resources*. doi: 10.1016/j.advwatres.2012.07.023.

Feddes, R., Kowalik, P., and Zaradny, H. (1978) 'Simulation of field water use and crop yield., Simulation Monograph Series', Pudoc, Wageningen, the Netherlands.

Francia, E., Tondelli, A., Rizza, F., Badeck, F. W., Nicosia, O. L. D., Akar, T., Grando, S., Al-Yassin, A., Bendelkacem, A., Thomas, W. T. B., van Eeuwijk, F., Romagosa, I., Stanca, A. M. and Pechhioni, N. (2011) 'Determinants of barley grain yield in a wide range of Mediterranean environments', *Field Crops Research*. doi: 10.1016/j.fcr.2010.09.010.

Gale, M. R. and Grigal, D. F. (1987) 'Vertical root distributions of northern tree species in relation to successional status', *Can. J. For. Res.*, 17, pp. 829–834.

García Ben, M. and Yohai, V. J. (2004) 'Quantile-quantile plot for deviance residuals in the generalized linear model', *Journal of Computational and Graphical Statistics*. doi: 10.1198/1061860042949_a.

Gebler, S., Hendricks Franssen H. -J., Pütz, T., Post, H., Schmidt, M. and Vereecken, H. (2015) 'Actual evapotranspiration and precipitation measured by lysimeters: A comparison with eddy covariance and tipping bucket', *Hydrology and Earth System Sciences*, 19(5), pp. 2145–2161. doi: 10.5194/hess-19-2145-2015.

Gilgen, A. K. and Buchmann, N. (2009) 'Response of temperate grasslands at different altitudes to simulated summer drought differed but scaled with annual precipitation', *Biogeosciences*. doi: 10.5194/bg-6-2525-2009.

Gill, J. S., Sivasithamparam, K. and Smettem, K. R. J. (2000) 'Soil types with different texture affects development of Rhizoctonia root rot of wheat seedlings', *Plant and Soil*. doi: 10.1023/A:1004606016745.

Giorgi, F. and Lionello, P. (2008) 'Climate change projections for the Mediterranean region', *Global and Planetary Change*. doi: 10.1016/j.gloplacha.2007.09.005.

Goffe, W. L., Ferrier, G. D. and Rogers, J. (1994) 'Global optimization of statistical functions with simulated annealing', *Journal of Econometrics*. doi: 10.1016/0304-4076(94)90038-8.

Gupta, H. V, Beven, K. J. and Wagener, T. (2005) 'Model Calibration and Uncertainty Estimation', in *Encyclopedia of Hydrological Sciences*. doi: 10.1002/0470848944.hsa138.

Heathman, G. C., Starks, P. J., Ahuja, L. R. and Jackson, T. J. (2003) 'Assimilation of surface soil moisture to estimate profile soil water content', *Journal of Hydrology*. doi: 10.1016/S0022-1694(03)00088-X.

Hendricks Franssen H. -J., Stöckli, R., Lehner, I., Rotenberg, E. and Seneviratne, S. I. (2010) 'Energy balance closure of eddy-covariance data: A multisite analysis for European FLUXNET stations', *Agricultural and Forest Meteorology*. doi: 10.1016/j.agrformet.2010.08.005.

Huang, Y., Hendricks Franssen H. -J., Herbst, M., Hirschi, M., Michel, D., Seneviratne, S. I., Teuling, A. J., Vogt, R., Detlef, S., Pütz, T. and Vereecken, H. (2020) 'Evaluation of different methods for gap filling of long-term actual evapotranspiration time series measured by lysimeters', *Vadose Zone Journal*. doi: 10.1002/vzj2.20020.

Ivanov, V. Y., Bras, R. L. and Vivoni, E. R. (2008) 'Vegetation-hydrology dynamics in complex terrain of semiarid areas: 1. A mechanistic approach

to modeling dynamic feedbacks', *Water Resources Research*, 44(3). doi: 10.1029/2006WR005588.

Jackson, R. B., Canadell, J., Ehleringer, J. R., Mooney, H. A., Sala, O. E. and Schulze, E. D. (1996) 'A global analysis of root distributions for terrestrial biomes', *Oecologia*, 108(3), pp. 389–411. doi: 10.1007/BF00333714.

Jarvis, N. (2010) 'Comment on "Macroscopic Root Water Uptake Distribution Using a Matric Flux Potential Approach"', *Vadose Zone Journal*. doi: 10.2136/vzj2009.0148.

Jarvis, N., Koestel, J., Messing, I., Moeys, J. and Lindahl, A. (2013) 'Influence of soil, land use and climatic factors on the hydraulic conductivity of soil', *Hydrology and Earth System Sciences*, 17(12), pp. 5185–5195. doi: 10.5194/hess-17-5185-2013.

Jarvis, N. J. (1989) 'A simple empirical model of root water uptake', *Journal of Hydrology*. doi: 10.1016/0022-1694(89)90050-4.

Jarvis, N. J. (2011) 'Simple physics-based models of compensatory plant water uptake: Concepts and eco-hydrological consequences', *Hydrology and Earth System Sciences*. doi: 10.5194/hess-15-3431-2011.

Kampf, S. K. and Burges, S. J. (2010) 'Quantifying the water balance in a planar hillslope plot: Effects of measurement errors on flow prediction', *Journal of Hydrology*. doi: 10.1016/j.jhydrol.2009.10.036.

Kobayashi, S. and Maruyama, T. (1976) 'Search for the Coefficients of the Reservoir Model with the Powell's Conjugate Direction Method', (In Japanese, with English abstract.) *Transactions of the Japanese Society of Irrigation, Drainage and Reclamation Engineering*.

Lai, C. T. and Katul, G. (2000) 'The dynamic role of root-water uptake in coupling potential to actual transpiration', *Adv. Water Resour.*, 23, pp. 427–439.

Li, K. Y., De, Jong, R., Coe, M. T., and Ramankutty, N. (2006) 'Root-water uptake based upon a new water stress reduction and an asymptotic root distribution function', *Earth Interact.*, 10, pp. 1–22.

Li, S., Kang, S., Zhang, L., Li, F., Zhu, Z. and Zhang, B. (2008) 'A comparison of three methods for determining vineyard evapotranspiration in the arid desert regions of northwest China', *Hydrological Processes*. doi: 10.1002/hyp.7059.

López-Urrea, R., Martín de Santa Olalla, F., Fabeiro, C. and Moratalla, A. (2006) 'An evaluation of two hourly reference evapotranspiration equations for

semiarid conditions', *Agricultural Water Management*. doi: 10.1016/j.agwat.2006.05.017.

Meissner R., Prasad M. N. V., Du Laing G., Rinklebe J. (2010) 'Lysimeter application for measuring the water and solute fluxes with high precision', *Current Science,* 99 (5), pp. 601-607.

Meissner, R., Seeger, J., Rupp, H., Seyfarth, M. and Borg, H. (2007) 'Measurement of dew, fog, and rime with a high-precision gravitation lysimeter', *Journal of Plant Nutrition and Soil Science*. doi: 10.1002/jpln.200625002.

Miles, J. (2014) 'R Squared, Adjusted R Squared', in *Wiley StatsRef: Statistics Reference Online*. doi: 10.1002/9781118445112.stat06627.

Morecroft, M. D., Masters, G. J., Brown, V. K., Clarke, I. P., Taylor, M. E. and Whitehouse, A. T. (2004) 'Changing precipitation patterns alter plant community dynamics and succession in an ex-arable grassland', *Functional Ecology*. doi: 10.1111/j.0269-8463.2004.00896.x.

NASA JPL (2013). NASA Shuttle Radar Topography Mission Global 1 arc second. NASA EOSDIS Land Processes DAAC. Accessed 2020-02-07 from https://doi.org/10.5067/MEaSUREs/SRTM/SRTMGL1.003.

Olesen, J. E., Trnka, M., Kersebaum, K. C., Skjelvåg, A. O., Seguin, B., Peltonen-Sainio, P., Rossi, F., Kozyra, J. and Micale, F. (2011) 'Impacts and adaptation of European crop production systems to climate change', *European Journal of Agronomy*. doi: 10.1016/j.eja.2010.11.003.

Pallant, J. (2007) 'SPSS survival manual, 3rd', *Edition. McGrath Hill*.

Peters, A., Nehls, T., Schonsky, H. and Wessolek, G. (2014) 'Separating precipitation and evapotranspiration from noise - A new filter routine for high-resolution lysimeter data', *Hydrology and Earth System Sciences*. doi: 10.5194/hess-18-1189-2014.

Pinheiro, E. A. R., van Lier, Q. D. J., and Metselaar, K. (2018) 'A Matric Flux Potential Approach to Assess Plant Water Availability in Two Climate Zones in Brazil', *Vadose Zone Journal*. doi: 10.2136/vzj2016.09.0083.

Powell, M. J. D. (1964) 'An efficient method for finding the minimum of a function of several variables without calculating derivatives', *The Computer Journal*. doi: 10.1093/comjnl/7.2.155.

Richards, L. A. (1931) 'Capillary conduction of liquids through porous mediums', *Journal of Applied Physics*. doi: 10.1063/1.1745010.

Pütz, T., Kiese, S., Wollschläger, Groh, J., Rupp, H., Zacharias, S., Priesack, E., Gerke, H. H., Gasche, R., Bens, O., Borg, E., Baessler, C., Kaiser, K., Herbrich, M., Munch, J. -C., Sommer, M., Vogel, H. -J., Vanderborght, J. and Veereecken, H. (2016) 'TERENO-SOILCan: a lysimeter-network in Germany observing soil processes and plant diversity influenced by climate change', *Environmental Earth Sciences*, 75(18). doi: 10.1007/s12665-016-6031-5.

Raats, P. A. C. (2007) 'Uptake of water from soils by plant roots', *Transport in Porous Media*. doi: 10.1007/s11242-006-9055-6.

Ren, Z. and Li, M. (2007) 'Errors and correction of precipitation measurements in China.', *Adv. Atmos. Sci.*, 24(3), pp. 449–458. doi: https://doi.org/10.1007/s00376-007-0449-3.

Rosopa, P. J., Schaffer, M. M. and Schroeder, A. N. (2013) 'Managing heteroscedasticity in general linear models', *Psychological Methods*. doi: 10.1037/a0032553.

Running, S. W. and Kimball, J. S. (2005) 'Satellite-Based Analysis of Ecological Controls for Land-Surface Evaporation Resistance', in *Encyclopedia of Hydrological Sciences*. doi: 10.1002/0470848944.hsa110.

Sánchez, P. J. (2006) 'As simple as possible, but no simpler: A gentle introduction to simulation modeling', in *Proceedings - Winter Simulation Conference*. doi: 10.1109/WSC.2006.323033.

Santos, M. A., van Lier, Q. D. J., van Dam, J. C. and Bezerra, A. H. F. (2017) 'Benchmarking test of empirical root water uptake models', *Hydrology and Earth System Sciences*, 21(1), pp. 473–493. doi: 10.5194/hess-21-473-2017.

Sawada, Y. and Toshio, K. (2014) 'Simultaneous estimation of both hydrological and ecological parameters in an ecohydrological model by assimilating microwave signal', *Journal of Geophysical Research (Atmospheres)*, 119(10), pp. 8839–8857. doi: 10.1002/2014JD021606.

Schaap, M. G. and Leij, F. J. (2000) 'Improved Prediction of Unsaturated Hydraulic Conductivity with the Mualem-van Genuchten Model', *Soil Science Society of America Journal*. doi: 10.2136/sssaj2000.643843x.

Sevruk, B. (1996) 'Adjustment of tipping-bucket precipitation gauge measurements', *Atmospheric Research*. doi: 10.1016/0169-8095(95)00066-6.

Sevruk, B., Hertig, J. A. and Spiess, R. (1991) 'The effect of a precipitation gauge orifice rim on the wind field deformation as investigated in a wind tunnel',

Atmospheric Environment Part A, General Topics. doi: 10.1016/0960-1686(91)90228-Y.

Silva, A. J. P. and Coelho, E. F. (2014) 'Estimation of water percolation by different methods using TDR', *Revista Brasileira de Ciência do Solo*. doi: 10.1590/s0100-06832014000100007.

Šimůnek, J., van Genuchten, M. T. and Sejna, M. (2011) 'The HYDRUS Software Package for Simulating the Two- and Three-Dimensions Movement of Water, Heat, and Multiple Solutes in Variably-Saturated Media', *Technical Manual*. doi: 10.1007/SpringerReference_28001.

Šimůnek, J., van Genuchten, M. T. and Wendroth, O. (1998) 'Parameter Estimation Analysis of the Evaporation Method for Determining Soil Hydraulic Properties', *Soil Science Society of America Journal*. doi: 10.2136/sssaj1998.03615995006200040007x.

Strangeways, I. C. (1996) 'Back to basics: The "met. enclosure": Part 2(b) — raingauges, their errors', *Weather*. doi: 10.1002/j.1477-8696.1996.tb06230.x.

Trnka, M., Olesen, J. E., Kersebaum, K. C., Skjevåg, A. O., Eitzinger, J., Seguin, B., Peltonen-Sainio, P., Rötter, R., Iglesias, A., Orlandini, S., Dubrovský, M., Hlavinka, P., Balek, J., Eckersten, H., Cloppet, E., Calanca, P., Gobin, A., Vučetić, V., Nejedlik, P., Kumar, S., Lalic, B., Mestre, A., Rossi, F., Kozyra, J., Alexandrov, V., Semerádová, D. and Žalud, Z. (2011) 'Agroclimatic conditions in Europe under climate change', *Global Change Biology*. doi: 10.1111/j.1365-2486.2011.02396.x.

van Genuchten, M. T. (1980) 'A Closed-form Equation for Predicting the Hydraulic Conductivity of Unsaturated Soils', *Soil Science Society of America Journal*, 44(5), pp. 892–898. doi: 10.2136/sssaj1980.03615995004400050002x.

van Lier, Q. D. J., van Dam, J. C., Metseelar, K., de Jong, K. and Duijnisveld, W. H. M. (2008) 'Macroscopic Root Water Uptake Distribution Using a Matric Flux Potential Approach', 7(3). doi: 10.2136/vzj2007.0083.

van Lier, Q. D. J., Neto, D. D. and Metselaar, K. (2009) 'Modeling of transpiration reduction in van genuchten-mualem type soils', *Water Resources Research*, 45(2), pp. 1–9. doi: 10.1029/2008WR006938.

van Lier, Q. D. J., Metselaar, K. and van Dam, J. C. (2006) 'Root Water Extraction and Limiting Soil Hydraulic Conditions Estimated by Numerical Simulation', *Vadose Zone Journal*. doi: 10.2136/vzj2006.0056.

von Unold, G. and Fank, J. (2008) 'Modular design of field lysimeters for specific application needs', *Water, Air, and Soil Pollution: Focus*, 8(2), pp. 233–242. doi: 10.1007/s11267-007-9172-4.

Vaughan, P. J., Trout, T. J. and Ayars, J. E. (2007) 'A processing method for weighing lysimeter data and comparison to micrometeorological ETo predictions', *Agricultural Water Management*. doi: 10.1016/j.agwat.2006.10.008.

Vinnikov, K. Y., Robock, A., Qui, S., Entin, J. K., Owe, M., Choudhury, B. J., Hollinger, S. E. and Njoku, E. G. (1999) 'Satellite remote sensing of soil moisture in Illinois, United States', *Journal of Geophysical Research Atmospheres*. doi: 10.1029/1998JD200054.

Wallace, J. S. (2000) 'Increasing agricultural water use efficiency to meet future food production', *Agriculture, Ecosystems and Environment*. doi: 10.1016/S0167-8809(00)00220-6.

White, K. L. and Chaubey, I. (2005) 'Sensitivity analysis, calibration, and validations for a multisite and multivariable SWAT model', *Journal of the American Water Resources Association*. doi: 10.1111/j.1752-1688.2005.tb03786.x.

Wriedt, G. (2004) '*Modelling of nitrogen transport and turnover during soil and groundwater passage in a small lowland catchment of Northern Germany*', *Mathematisch-Naturwissenschaftlichen Fakultät*.

Xu, J., Peng, S., Luo, Y. and Wei, Z. (2009) 'Influences of angstrom's coefficients on estimate of solar radiation and reference evapotranspiration by penman-monteith equation', in *Advances in Water Resources and Hydraulic Engineering - Proceedings of 16th IAHR-APD Congress and 3rd Symposium of IAHR-ISHS*. doi: 10.1007/978-3-540-89465-0_61.

Yang, D., Ishida, S., Goodison, B. E. and Gunther, T. (1999) 'Bias correction of daily precipitation measurements for Greenland', *Journal of Geophysical Research Atmospheres*. doi: 10.1029/1998JD200110.

Zacharias, S., Bogena, H., Samaniego, L., Mauder, M., Fuß, R., Pütz, T., Frenzela, M., Schwanke, M., Baesslera, C., Butterbach-Bahlc, K., Bense, O., Borgf, E., Brauere, A., Dietricha, P., Hajnsekg, I., Hellef, G., Kiesec, R., Kunstmannc, H., Klotza, S., Munchd, J. C., Papenc, H., Priesackd, E., Schmidc, H. P., Steinbrecherc, R., Rosenbaumb, U., Teutscha, G. and Vereecken, H. (2011) 'A network of terrestrial environmental observatories in Germany', Vadose Zone J. 10: pp. 955–973. doi:10.2136/vzj2010.0139

Zebisch, M., Grothmann, T., Schröter, D., Hasse, C., Fritsch, U. and Cramer, W. (2005) 'Climate change in Germany—vulnerability and adaptation of

climate sensitive sectors', Research Report 201 41 253 UBA-FB 000844/e. Federal Environmental Agency (Umweltbundesamt), P.O. Box 1406, D-06844 Dessau

Zheng, F. L. (2006) 'Effect of Vegetation Changes on Soil Erosion on the Loess Plateau', Pedosphere. doi: 10.1016/s1002-0160(06)60071-4.

Acknowledgements

Appendix

Appendix A – Calculation of net longwave radiation for FAO-56 Penman-Monteith equation

$$R_{so} = (0.75 + 2 \cdot 10^{-5} \cdot z) \cdot R_a \tag{A1}$$

R_{so} = Calculated clear-sky radiation [MJ m^{-2} day^{-1}]
z = Station elevation above sea level [m]
R_a = Extraterrestrial radiation [MJ m^{-2} day^{-1}]

$$R_a = \frac{12 \cdot 60}{\pi} G_{sc} \cdot d_r [(\omega_s \cdot sin\varphi \cdot sin\delta) + (cos\varphi \cdot cos\delta \cdot sin\omega_s)] \tag{A2}$$

R_a = Extraterrestrial radiation [MJ m^{-2} day^{-1}]
G_{sc} = solar constant = 0.0820 [MJ m^{-2} min^{-1}]
d_r = inverse relative distance Earth-Sun [-]
ω_s = sunset hour angle [rad]
φ = Latitude [rad]
δ = Solar declination [rad]

$$d_r = 1 + 0.033 cos \left[\frac{2\pi}{365} \cdot J \right] \tag{A3}$$

d_r = inverse relative distance Earth-Sun [-]
J = Julian day, number of day in a year [-]

$$\delta = 0.409 sin \left[\frac{2\pi}{365} \cdot J - 1.39 \right] \tag{A4}$$

δ = Solar declination [rad]
J = Julian day, number of day in a year [-]

$$\omega_s = arccos [-tan(\varphi)tan(\delta)] \tag{A5}$$

ω_s = sunset hour angle [rad]
φ = Latitude [rad]
δ = Solar declination [rad]

Appendix B – Calibration steps

The algorithm starts to search for the point x_1 in the conjugate direction d_1 starting from the initial point x_0, followed by calculation of $f(x_1)$. Further, Powell's method search for the local minimum point x_i in conjugate direction d_i from initial point x_{i-1} and calculates $f(x_i)$. Then it sets $f_1 = f(x_0)$ and $f_2 = f(x_n)$ and calculates $f_3 = f(2x_n-x_0)$. Lately, method sets $m = i$ and calculates the maximum value of equation A6.

$$|f(x_{(i-1)}) - f(x_i)| \tag{A6}$$

In a case, if the assumption in equation A7 is met, the algorithm moves to the next step seen in equation A10. Otherwise, the method follows equations A8 and A9 and starts a search in conjugate direction d_n for a local minimum value $x_{0(new)}$ from the point x_n.

$$x_{0(new)} - x_n \quad ; f_3 \geq f_1 \tag{A7}$$

$$d_{m+i} = d_{m+i+1} \ ; f_3 < f_1 \tag{A8}$$

$$d_n = \frac{x_n - x_0}{|x_n - x_0|} ; f_3 < f_1 \tag{A9}$$

If the assumption in equation A10 is met, then the local minimum point is obtained while in the opposite case when equation A10 is greater than convergence criterion (ε) then $x_0 = x_{0(new)}$ and algorithm repeat calculations from the initial step.

$$x_{0(new)} \quad ; |x_{0(new)} - x_0| \leq \varepsilon \tag{A10}$$

According to Chen, Pi and Hsieh, (2005) application of Powell's method to solve multiple optimum problems through repeating search from different starting points allowed to combine this algorithm with "multistart" procedure by determining a number of search points (z) and selecting the search point corresponding conditions from the search space with random selection followed by point search with Powell's method. During the search, the process penalty function is adopted to exclude selection of unreasonable parameter values. Further, steps are repeated n times and best values are stored in the matrix with the final selection of the smallest function value.